Posted on 26 Nov 2022 — The copyright holder is the author/funder. All rights reserved. No reuse without permission. — https://doi.org/10.1002/essoar.10506643.1 — This a preprint and has not been peer reviewed. Data may be preliminary.

Effect of lateral and temporal viscosity variations on GIA induced uplift rates in the Amundsen Sea Embayment

Bas Blank[1], Valentina Roberta Barletta[2], Haiyang X. S. Hu[1], Folker Pappa[3], and Wouter van der Wal[1]

[1]Delft University of Technology
[2]DTU Space
[3]Kiel University

November 26, 2022

Abstract

Accurate GIA models are required for correcting measurements of mass change in Antarctica and for improving our knowledge of the sub-surface, especially in areas of large current ice loss such as the Amundsen Sea Embayment. There, seismic and gravity data suggests lateral differences in viscosity. Furthermore, mantle flow laws allow for time-varying viscosity. In this study we investigate whether spatial and temporal variations in viscosity (4D viscosity) have significant effects on the measured uplift in the region. We use a finite element model with composite rheology consisting of diffusion on and dislocation creep, forced by an ice deglaciation model starting in 1900. We use its uplift predictions as synthetic observations to test the performance of 1D model inversion in the presence of viscosity variations. Introducing time-varying viscosity results in lower viscosity beneath the load and a more localized uplift pattern. We demonstrate that the background stress from earlier ice load changes, can increase and decrease the influence of stress-induced viscosity changes. For the ASE, fitting 1D models to 3D model uplift results in a best fitting model with viscosity that is equal to the average of a large contributing area, while for 4D the local viscosity is more crucial. 1D models are statistically indistinguishable from 3D/4D models with current GPS stations. However, 3D and 4D models should be taken into account when accurate uplift and gravity rate patterns are needed for correcting satellite measurements or predicting relaxation times, as uplift can differ up to 45\% compared to 1D models.

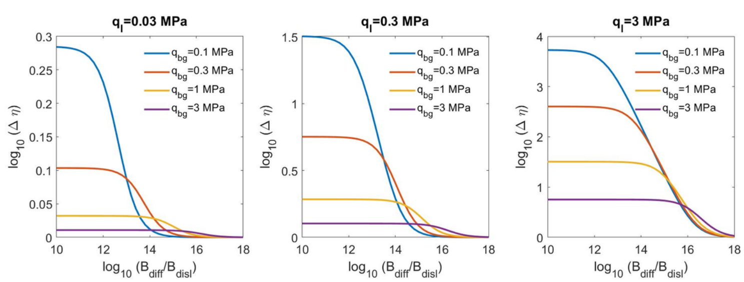

Posted on 26 Nov 2022 — The copyright holder is the author/funder. All rights reserved. No reuse without permission. — https://doi.org/10.1002/essoar.10506643.1 — This a preprint and has not been peer reviewed. Data may be preliminary.

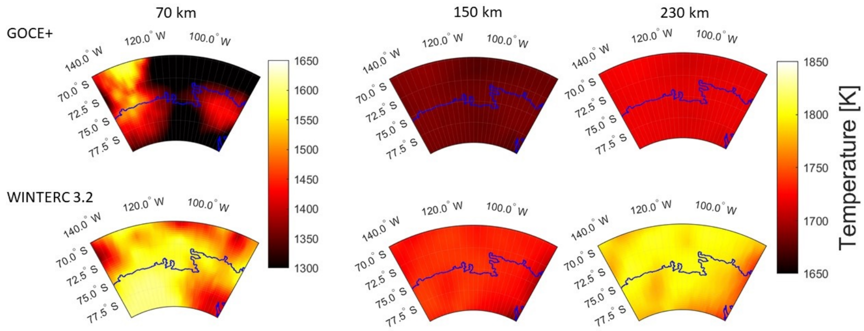

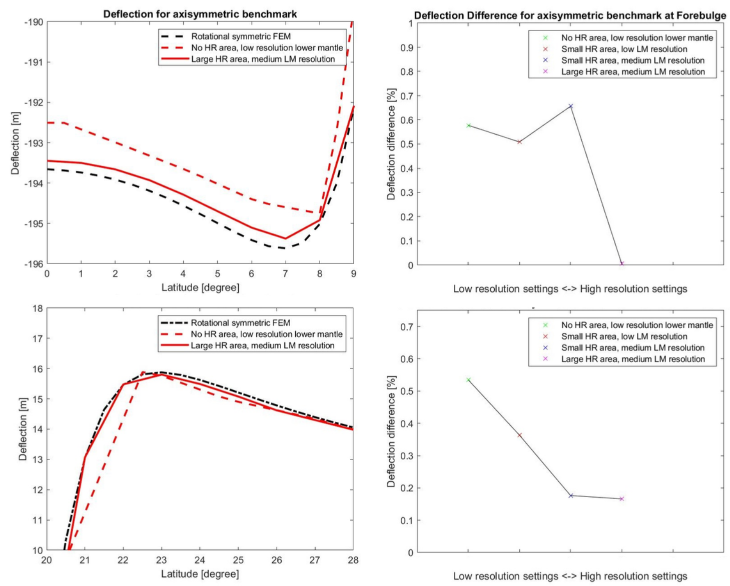

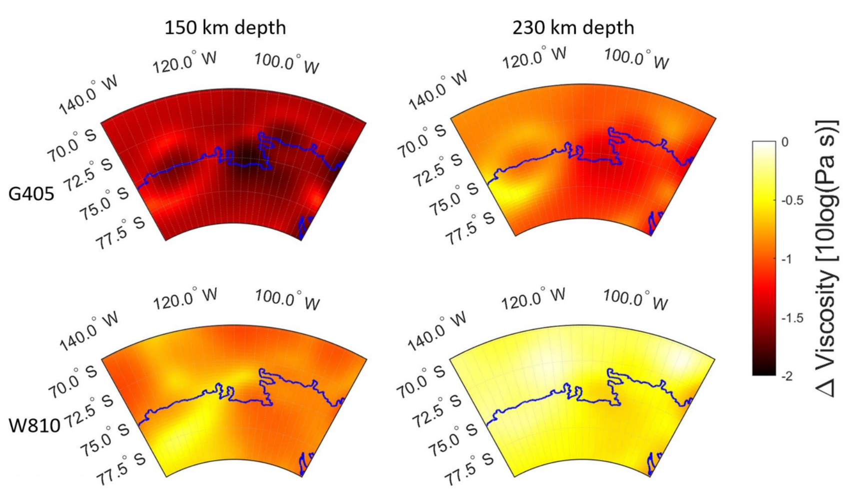

Effect of lateral and temporal viscosity variations on GIA induced uplift rates in the Amundsen Sea Embayment

B. Blank[1], V. Barletta[2], H. Hu[3], F. Pappa[4], and W. van der Wal[1]

[1]University of Technology Delft, Kluyverweg 1, Delft, The Netherlands
[2]University of Technology Denmark, Anker Engelunds Vej 1 Bygning 101A, Kgs. Lyngby, Denmark
[3]Imperial College London, South Kensington, Londen, England
[4]Kiel University, Otto-Hahn-Platz 1, Kiel, Germany

Key Points:

- Uplift rates due to ice thickness changes in ASE since 1900 is modeled with lateral and temporal (4D) viscosity changes based on composite rheology.
- Including stresses from earlier ice loads can both increase and decrease the influence of stress-induced viscosity changes.
- 1D models can not be distinguished from 4D models in a misfit analysis with the current GPS station distribution, but uplift rates differ significantly locally.

Corresponding author: Bas Blank, `b.blank@tudelft.nl`

Abstract

Accurate GIA models are required for correcting measurements of mass change in Antarctica and for improving our knowledge of the sub-surface, especially in areas of large current ice loss such as the Amundsen Sea Embayment. There, seismic and gravity data suggests lateral differences in viscosity. Furthermore, mantle flow laws allow for time-varying viscosity. In this study we investigate whether spatial and temporal variations in viscosity (4D viscosity) have significant effects on the measured uplift in the region. We use a finite element model with composite rheology consisting of diffusion on and dislocation creep, forced by an ice deglaciation model starting in 1900. We use its uplift predictions as synthetic observations to test the performance of 1D model inversion in the presence of viscosity variations. Introducing time-varying viscosity results in lower viscosity beneath the load and a more localized uplift pattern. We demonstrate that the background stress from earlier ice load changes, can increase and decrease the influence of stress-induced viscosity changes. For the ASE, fitting 1D models to 3D model uplift results in a best fitting model with viscosity that is equal to the average of a large contributing area, while for 4D the local viscosity is more crucial. 1D models are statistically indistinguishable from 3D/4D models with current GPS stations. However, 3D and 4D models should be taken into account when accurate uplift and gravity rate patterns are needed for correcting satellite measurements or predicting relaxation times, as uplift can differ up to 45% compared to 1D models.

Plain Language Summary

The Amundsen Sea Embayment (ASE) is a region in West-Antarctica, which is melting faster than almost any other region It is critical to know how much the area is currently melting. However, measurements of current ice mass change are obscured by uplift due to the melting of ice sheets in that past, termed Glacial Isostatic Adjustment (GIA). An accurate GIA model is required. The state-of-the-art GIA model for the region assumes that the viscosity depth profile is the same everywhere. However, viscosity can change with location and also over time. In this study we use a finite element model to simulate GIA in the ASE and compare these results to simulated uplift from a 1D model. We show that when estimating average viscosities in the mantle a simpler model would suffice. When higher stresses due to rapid deglaciation are taken into account in the description of the mantle flow the uplift at the point of rapid deglaciation has a stronger rebound effect than previously considered. This would mean that the local ice mass loss obtained after correcting with current GIA models might also be bigger then what is obtained after correcting ice mass change measurements with simpler GIA models.

1 Introduction

Glacial isostatic adjustment (GIA) is the response of the solid Earth to changes in the ice sheet. It is ongoing in areas of former large Pleistocene ice sheets such as North America and Scandinavia, but also in currently glaciated areas such as Antarctica. There, modelling of GIA is necessary to correct satellite measurements of mass change for GIA in order to reveal current ice mass change (King et al., 2010; Shepherd et al., 2019; Caron & Ivins, 2020). Additionally, comparing output of GIA models to observations that are dominated by GIA or corrected for current ice mass change effects can give us insight in the structure of the Earth. GIA is sensitive to a viscosity distribution in radial direction, but also in longitudinal and lateral directions. This is particularly relevant in Antarctica, where it is known that a large contrast between East and West Antarctic mantle exists. Furthermore, GIA plays an important role in the deglaciation process itself through a feedback loop of the solid-earth response with the Antarctic ice sheet (Gomez et al., 2018; Barletta et al., 2018; Whitehouse et al., 2019). Still 1D models (Whitehouse et al., 2012; Ivins et al., 2013; Peltier, 2004) have mostly been used to correct satellite gravimetry measurements (King et al., 2010; Shepherd et al., 2019) because of their computational simplicity. 1D models have also been used to model small regions in West-Antarctica which have lower than average viscosity (Nield et al., 2014; Wolstencroft et al., 2015; Samrat et al., 2020).

GIA induced uplift rate and horizontal rate is altered when using 3D rheology (Kaufmann et al., 2005; A et al., 2013; van der Wal et al., 2015; Nield et al., 2018), especially near the boundary between low viscosities in west-Antarctica and high viscosities in East-Antarctica. In Kaufmann et al. (2005) a 3D model was used to investigate the effects of the lateral viscosity variations in the Antarctic mantle. While the results of Kaufmann et al. (2005) showed that their 3D Maxwell rheology has some influence on GIA (most notably horizontal motion), they concluded that the differences in ice models have a larger impact. In A et al. (2013) a compressible 3D rheology was used to show that the inclusion of a 3D rheology influences GIA model predictions can have a large effect on the uplift in Antarctica (up to 60%), but this was when comparing local uplift with an Antarctica wide viscosity average. On top of that the difference for the ASE specifically were very small to non at all. However, as these studies were not focussed on rheology, both Kaufmann et al. (2005) and A et al. (2013) tested a single set of 3D rheology parameters and used ice models that did not incorporate the large recent ice loss in the ASE. It is shown by van der Wal et al. (2015) using multiple different sets of rheology parameters that the effect of unknown lateral viscosity changes can be larger than these previous studies suggested. This raises the question under what condition 3D viscosity variations become significant.

The Amundsen Sea Embayment (ASE) exhibts the largest observed ice mass loss of the Antarctic continent in the last few decades (Martín-Español, Zammit-Mangion, et al., 2016; Gunter et al., 2014) of about -130Gt/y (Barletta et al., 2018). A destabilization of the Amundsen glaciers could start a collapse of the whole West-Antarctic ice sheet (Fledmann & Levermann, 2015) even though solid earth response could provide a positive feedback that acts to slow down the acceleration of ice melt (Konrad et al., 2015). The largest ice loss currently occurs at the Pine Island Glacier (PIG), the glaciers near the Crosson Ice shelf and at the Thwaites Glacier (TG) (Gourmelen et al., 2018; Konrad et al., 2016). The ASE is the region where the highest uplift is measured by means of GPS stations. Only a small part of the uplift rates is explained by present-day melt, which indicates that the region either has an ice history in which large Pleistocene or early Holocene loads were present or it is underlain by a low viscosity which makes it more sensitive to more recent ice load changes. Global or large scale GIA models (Nield et al., 2018; Martín-Español, King, et al., 2016) (either 3D or 1D) are unable to predict the GPS measured uplift values observed in the ASE because they do not model the deglaciation in the last century. Barletta et al. (2018) demonstrated with a 1D model that the ice loss of the last few decades in combination with a low viscosity is necessary to explain the high uplift values.

In Barletta et al. (2018), a good fit was achieved between GPS data and simulations with a GIA model in which viscosity only varies in radial direction. However, seismic models suggest changes in Earth properties below or near the region (An et al., 2015a; Lloyd et al., 2015) but it is not known if these viscosity contrasts have significant effects on the uplift rate. Furthermore, it is not clear whether the viscosities found for the ASE by means of a 1D model are a good representation of the average 3D viscosity, and whether inferences from 1D models can be used as local constraints on 3D viscosity maps. Viscosity is a macroscopic description of deformation that takes place at micro-scale. Experiments on mantle rocks show different deformation mechanisms which depend on the grain size of the rock, but also mechanisms which depend on stress with an exponent larger than one (Hirth & Kohlstedt, 2003). Such behaviour can be described as power-law rheology and it is non-linear in nature.

Nield et al. (2018) showed that the use of a representative 1D model may not only affect the magnitude of the GIA uplift compared to 3D non-linear rheology, but also the uplift gradient in their GIA uplift profile. Non-linear rheology results in steeper gradient and makes the pattern more localized. More recently there have even been efforts through the combination of multiple 1D models, to simulate 3D lateral differences in Earth structure. In Hartmann et al. (2020) Antarctica was modelled by different 1D models for the Eastern and Western parts of the continent. The results showed large conformity with the 3D finite volume model used in (Hay et al., 2017). Finally, in Powell et al. (2020) a direct comparison is made between 3D models and 1D models for Antarctica and West-Antarctica specifically. Their conclusion is that introducing lateral viscosity differences lead to measurable differences in horizontal bedrock movement and little to no difference with respect to the vertical component for the stations in ASE. However, there is strong emphasis on recent ice mass solely which leaves the question how past changes in both ice loading and Earth parameters might affect their conclusions

Using power-law rheology the viscosity becomes stress-dependent, with higher stresses causing lower viscosity. Therefore, large ice mass changes and the subsequent stress changes can lower local viscosity. Furthermore, in a power-law rheology viscosity is also dependent on background stresses (Schmeling, 1987; Gasperini et al., 1992; Wu, 2001). To express the fact that viscosity changes with location and time, we will use the term 4D viscosity. 4D rheology is not widely considered when computing GIA corrections although the effect of time-varying viscosity is up to two order of magnitude in viscosity (Barnhoorn et al., 2011). A GIA model with stress-dependent viscosity has been used for Antarctica (van der Wal et al., 2015), but for the ASE there has been no study detailing the effect of non-linear rheology, and the effect on background stress.

We identified the following research question: *What is the influence of 3D/4D viscosity profiles in GIA models on uplift rates in the Amundsen Sea Sector?* This question is divided into the following sub-questions:

- How representative is the best fitting viscosity in a 1D Earth model of average 3D viscosity?
- Can 3D viscosity be discerned in current uplift rate measurements?
- How important is time-varying viscosity for the uplift?
- What is the influence of background stresses on time-varying viscosity and uplift?

In this study we will use 3D and 4D GIA models to simulate uplift rates at GPS station locations. The simulated GPS values will be used to perform an inversion for viscosity in a 1D model, similar to van der Wal et al. (2015). The best fitting 1D viscosities found will be compared to an average of the local 3D viscosities. This will provide insight in whether the best-fitting 1D viscosity model is an average of the 3D model, or whether it samples the 3D viscosities in a different way. Furthermore, we will also investigate the uplift pattern of the 3D and 4D models and see to what extent they can be represented by a 1D model. Finally, a comparison will be made between 3D and 4D models to study the effects of the stress-dependent viscosity. Here we also include a full glacial history to investigate whether the background stresses in the mantle due to earlier deglaciation influence our findings for the recent ice-load changes.

The structure of this paper is as follows. In section 2 we will start by introducing the FE model. After that, we will describe Earth model parameters and ice input for the model. This will be followed by a short description of the 1D model used for the inversion. In section 3 the research questions will be answered, after which main conclusions are summarized in the last section.

2 Method

2.1 3D finite element model

The 3D/4D model used in this study is a FE model based on the commercial software ABAQUS^{TM}, following the method of Wu (2004). In this approach a stress transformation is applied so that the equations of motion are transformed into a form in which they can be implemented in the FE model. Self-gravitation is applied by computing the change in gravitational potential and applying it to the model as a new force at each density interface after which a new deformation can be computed and the process is repeated until convergence. The FE model that formed the basis of the rotational dynamics model in Hu et al. (2017) has been modified to incorporate GIA, lateral varying viscosity, and variable resolution. A high resolution region (HRR) has been introduced to the model to simulate GIA in small regions, such as the ASE. A global model with high resolution is not computationally feasible. Therefore, the model was divided in sections with different element sizes, with the smallest elements located in the HRR around the ASE and larger elements located in the far-field (FF) (Figure 1). The element size of the far-field is based on similar models without HRR and a focus on continent scale GIA (van der Wal et al., 2015). Element sizes are given in Table 1. Furthermore, deeper layers such as the lower mantle are meshed with a lower resolution to further reduce the total amount of elements. Depending on the model the computation time of the model would be in the order of 5 to 10 days. A benchmark of the FE model in this configuration for different test cases can be found in the supplementary material. The code has been benchmarked with results from Martinec et al. (2018) for a spherical cap load near the north pole (64°N 75°W). It can be seen in figure **??** of the supplementary material that the deflection underneath and near ice masses differs between the FE model and the benchmark model 1.3% for a resolution of ± 0.25° x 0.25°. This is a significant improvement from the 2° x 2° of earlier implementations of the method of (Wu, 2004), including the 0.5° x 0.5° spatial resolution from the recent study of Huang et al. (2019). It must be noted that the resolution is lower when compared global to the finite volume models used in (Powell et al., 2020), or local normal mode model, such as (Barletta et al., 2018) whose grid points are approximately 5 km apart.

The sea-level equation (SLE) is included according to the algorithm from Kendall et al. (2005) including changes in shorelines due to melt-water influx and changing shorelines (Milne & Mitrovica, 1998; Johnston, 1993). Small changes to the algorithm of Kendall et al. (2005) are applied to make it suitable for the FEM; these can be found in the supplementary material. The effect of rotational feedback is small on the spatial scale that we consider and is not included. It is important to note that the sea-level equation can be solved at a higher resolu-

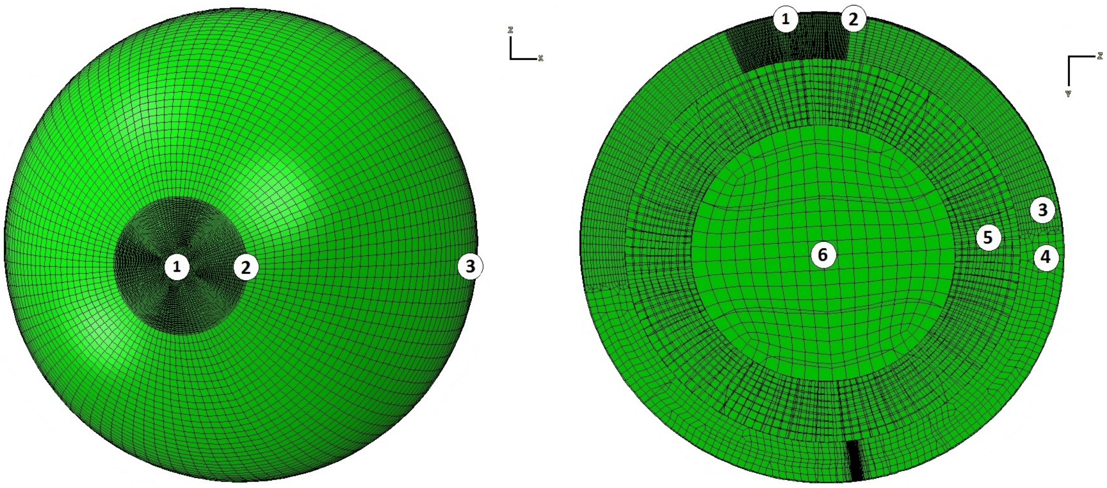

Figure 1. Finite-element mesh (left: top down view left, right: cross section view) used for the 3D FE GIA model. The high resolution area has a radius of 15 degrees (from point 1 to point 2) and is centered at the ASE (108.3°W, 76°S). Element dimensions for all six designated regions can be found in in Table 1.

tion than the FE grid. This allows shoreline locations which experience large force changes over time as a result of ice grounding to be modeled with high spatial accuracy. Here, the SLE is solved in a global equiangular grid of 0.25° x 0.25°. It must be noted that the full Sea level equation (SLE) is only used for the modelling of the ASE with a full glacial cycle ice history, to investigate the effect of Pleistocene ice history on present-day uplift rate and stress-dependent viscosity. For all other simulations a eustatic sea level with static shorelines is used to make the results comparable with a local 1D model.

Location	Latitudinal size [km]	Longitudinal size [km]	Radial size [km]
1. Center HRR	25	25	50
2. Rim HRR	27	92	50
3. FF south of equator	200	200	50
4. FF north of equator	200	200	200
5. Lower mantle	200	200	200
6. Core	400	400	400

Table 1. Approximate size of elements for sections of the model shown in figure 1, at the top of the specific layer .

2.2 Rheology

We assume that the rheology of the upper mantle is controlled by olivine and use the flow law compiled by Hirth and Kohlstedt (2003):

$$\dot{\epsilon} = Aq^n d^{-p} f_{H_2O}^r e^{\alpha\phi} e^{-\frac{E+PV}{RT}} \tag{1}$$

Here, A and α are experimentally determined constants. Furthermore, q represents the stress present. The parameter d represents the grain size, while f_{H_2O} represents the water content within the olivine. The parameter d and f_{H_2O} are considered to have the highest uncertainty and these will be used as free parameters that are varied between rheology models. The parameter ϕ is the melt fraction, we assume no melt in our rheology, so $\phi = 0$. Pressure P is assumed to increase linearly with depth Z according to $P(GPa) = 0.0333{\cdot}Z(km)$ (Kearey et al., 2009). R is the gas constant and T the local temperature. Temperature and stress are the only parameters that can vary with location, with temperature variations having a larger control on viscosity. Finally E is the activation energy and V is the activation volume.

The two main deformation mechanisms of olivine under upper mantle conditions are diffusion creep and dislocation creep. They can both be represented by equation 1. Diffusion creep rate is strongly dependent on grain size, with grain size exponent p of 3, but only linearly dependent on stress (stress exponent n of 1) and water content (water content exponent r of 1). Dislocation creep rate is linearly dependent on grain size ($p = 1$) and non-linearly dependent on stress ($n > 2$) and water content ($r = 1.2$). The non-linear stress-dependence gives rise to the time-dependence of viscosity. The deformation mechanisms have different activation energy and volume, as given in Hirth and Kohlstedt (2003). Following van der Wal et al. (2010) the two mechanisms are combined in a so-called composite rheology.

The olivine rheology is implemented in the FE model as follows. It is postulated that the relation between the stress and strain rate measured in a uni-axial experiment as compiled in Hirth and Kohlstedt (2003) also holds for the relation between the equivalent stress and equivalent strain rate (Ranalli, 1995):

$$\dot{\tilde{\epsilon}} = B\tilde{q}^n \tag{2}$$

where B is derived from equation 1

$$B = Ad^{-p} f_{H_2O}^r e^{\alpha\phi} e^{-\frac{E+PV}{RT}} \tag{3}$$

The equivalent stress used here is the so-called Von Mises stress:

$$\tilde{q} = \sqrt{\frac{3}{2}\mathbf{q}_{ij}\mathbf{q}_{ij}} \tag{4}$$

and the corresponding uni-axial equivalent strain rate is

$$\dot{\tilde{\epsilon}} = \sqrt{\frac{2}{3}\dot{\epsilon}_{ij}\dot{\epsilon}_{ij}} \tag{5}$$

To get a relation between tensor components, assume that the components of the deviatoric strain rate tensor are proportional to the components of the deviatoric stress tensor (Ranalli, 1995):

$$\dot{\epsilon}_{ij} = \lambda \mathbf{q}_{ij} \tag{6}$$

It can then be derived (van der Wal et al., 2013) that:

$$\dot{\epsilon}_{ij} = \frac{3}{2} B \tilde{q}^{n-1} \mathbf{q}_{ij} \tag{7}$$

In ABAQUS the uniaxial equivalent strain increments are computed as follows:

$$\Delta\tilde{\epsilon} = B\tilde{q}^{n}\Delta t \tag{8}$$

and components of the incremental strain tensor are computed as:

$$\Delta\epsilon_{ij} = \Delta\tilde{\epsilon}\frac{\delta\tilde{q}}{\delta\mathbf{q}_{ij}} \tag{9}$$

where the derivative is (Zhang, 2005):

$$\frac{\delta\tilde{q}}{\delta\mathbf{q}_{ij}} = \frac{3\mathbf{q}_{ij}}{2\tilde{q}} \tag{10}$$

Combining Equations 8-10 yields:

$$\Delta\epsilon_{ij} = \frac{3}{2} B \tilde{q}^{n-1} \mathbf{q}_{ij} \Delta t \tag{11}$$

which agrees with Equation 7. In ABAQUS, Equaton 8 is specified in user subroutine CREEP, where values for parameters B are read from a file with the user subroutine UEXTERNALDB. The stress transformation of Wu (2004) does not affect the deviatoric stress so the above equations can be used directly.

The equations in this section hold for both diffusion creep and dislocation creep. In order to implement the composite rheology we use the fact that diffusion creep and dislocation creep occur simultaneously and their components can be added for the uni-axial flow law and for the relation between the uni-axial equivalent strain rate and the Von Mises stress that is inputted in ABAQUS (Equation 8):

$$\Delta\epsilon_{ij} = \frac{3}{2}(B_{diff} + B_{disl}\tilde{q}^{n-1})\mathbf{q}_{ij}\Delta t \tag{12}$$

$$\dot{\tilde{\epsilon}} = \frac{3}{2}(B_{diff}\tilde{q} + B_{disl}\tilde{q}^{n})\Delta t \tag{13}$$

Defining an effective viscosity η_{eff} as $\eta_{eff} = \frac{\tilde{q}}{2\dot{\tilde{\epsilon}}}$, it follows from Equation 13 that (van der Wal et al., 2013)

$$\eta_{eff} = \frac{1}{3B_{diff} + 3B_{disl}\tilde{q}^{n-1}} \tag{14}$$

The viscosity depends directly on temperature estimates, and can vary strongly as a function of grain size and water content (Barnhoorn et al., 2011). This is in contrast to an approach whereby seismic velocity anomalies are scaled to viscosity anomalies (as for example done in Hay et al. (2017), Gomez et al. (2018) and Powell et al. (2020)). In that approach a background viscosity is needed, which can be selected from geodynamic studies. Our approach does not require a background viscosity model and can provide viscosity values that are independent from geodynamic studies. However, they depend strongly on grain size and water content which are unknown, and hence some constraints on these from other studies are necessary. In principal grain size and water content can also be varied with location but as we have little information on the grain size and water content across Antarctica van der Wal et al. (2015) they are kept spatially homogeneous. We have chosen the values based on a fit with GPS uplift values, as will be explained in the results section. For the areas outside of Antarctica we have chosen the diffusion creep parameter to be $1.11{\cdot}10^{-22}Pa^{-1}s^{-1}$ and the dislocation parameter to be $3.33{\cdot}10^{-35}Pa^{-3.5}s^{-1}$, with $n = 3.5$, which give good fit with global RSL data (van der Wal et al., 2010). This will effectively simulate a viscosity of $3.0 \cdot 10^{21} Pa \cdot s$ when no stress is considered. For the deeper mantle we considered a linear Maxwell rheology with a viscosity of $2 \cdot 10^{21} Pa \cdot s$

Equation 14 shows that the effective viscosity always decreases with an increased Von Mises stress. The affect of adding a predefined Von Mises stress in a non-linear rheology was investigated by Wu (2001) and for composite rheology by Gasperini et al. (1992). The main conclusion from these studies is that realistic predefined mantle stresses can significantly effect the GIA process, depending on their magnitude, as they impact the effective viscosity below the load over time.

In our composite rheology, the change in viscosity due to a load induced stress q_l in the presence of a background stress q_{bg} can be defined as follows:

$$\Delta\eta_{q_{bg}} = \frac{1}{3B_{diff} + 3B_{disl}q_{bg}^{n-1}} - \frac{1}{3B_{diff} + 3B_{disl}(q_{bg} + q_l)^{n-1}} \tag{15}$$

This equation depends on the importance of dislocation creep with respect to diffusion creep, and hence on the value of $\frac{B_{diff}}{B_{disl}}$ as well as the load induced stress. If we plot the results of Equation 15 for different values of q we can see aforementioned drop in effective viscosity in the presence of background stress as a function of $\frac{B_{diff}}{B_{disl}}$, see Figure 2. We see that for rheologies where the contribution of dislocation creep is large ($log10(B_{diff}/B_{disl}) = 10$), a large background stress will decrease the drop in viscosity as a consequence of the load induced stress. In these cases the viscosity is already lowered significantly by the background stress itself, so the extra

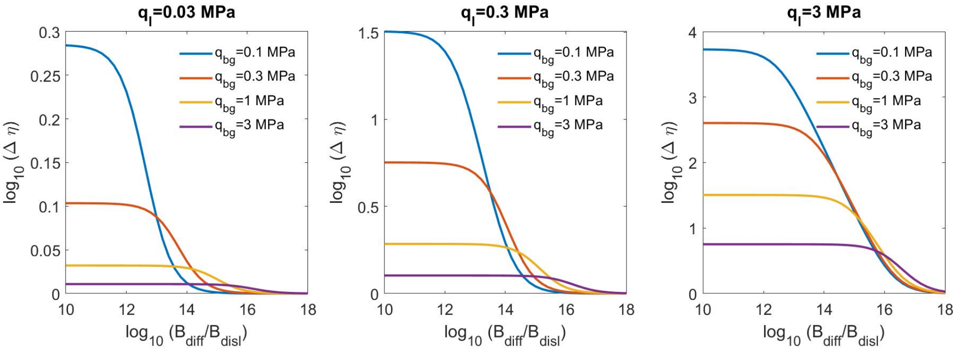

Figure 2. Decrease in viscosity $\log_{10}(\Delta\eta)$ as a function of different non-linear rheology settings B_{diff}/B_{disl} with different values of background stress q_{bg} present. Left: Drop in viscosity for different background stresses as a consequence of 30 kPa of load induced stress ($q_l = 0.03$ MPa). Centre: Drop in viscosity for different background stresses as a consequence of 0.3 MPa of load induced stress ($q_l = 0.3$ MPa). Right: Drop in viscosity for different background stresses as a consequence of 3 MPa of load induced stress ($q_l = 3$ MPa).

stress from the load has little impact. If on the other hand dislocation creep has a small contribution, the drop in viscosity caused by load induced stresses will always be low, regardless of background stress. In between the extreme cases there exists a window (around $log_{10}(B_{diff}/B_{disl}) \approx 13.5 - 18$ depending on the load magnitude) where larger background stresses will also lead to larger drops in viscosity when a load is applied. This window is relevant as it exist in the range of plausible rheologies. This means that, while the general rule is that the presence of background stress reduces the decrease in viscosity for a given load, in specific situations the presence of a background stress can also strengthen the effect of load induced stress and thus time dependancy for the solid earth response.

In reality the situation is more complicated because the Von Mises stress can both increase and decrease if a background stress field is added, depending on the magnitude and direction of the individual stress components (Schmeling, 1987). In section 3.4 we investigate the effect of stresses due to the response of the last glacial cycle on response due to recent ice loading. Both loading processes are simulated in the model, hence the stress addition takes place inside the FE model. This is the first time that the stress interaction from long timescale GIA and short timescale GIA are investigated.

Elastic parameters for the Earth model are the same as the M3-L70-V01 model (Spada et al., 2011) see Table 2. The entire model is assumed incompressible ($\nu = 0.5$). The top layer of the model is fully elastic and this layer is thinner (30 km) than the lithosphere in Spada et al. (2011) to allow for the fact that the elastic lithosphere can be thin in parts of Antarctica.

As a consequence the density of the top mantle layer has been adjusted to 3438 kg/m^3, to keep the total mass of the Earth constant. Below the crustal layer, the layers are visco-elastic and the effective viscosity determines whether there is significant viscous deformation over the time-scale of the loading. Thus, the elastic lithospheric thickness defined as the top part of the Earth that behaves fully elastic is defined implicitly by the effective viscosity. For the short loading scales of our study the lithospheric thickness will be larger than for a study for the full glacial cycle for the same Earth model (Nield et al., 2018). In the upper mantle, diffusion and dislocation creep parameters B are as calculated in Equation 3. The 3D variation in the creep parameters is determined by the temperature. Temperature estimates are discussed in the next section.

Layer	Depth top of layer (km)	Density (kg/m^3)	Youngs Modulus (Pa)	Viscosity ($Pa \cdot s$)
Crust	0	3037	$0.506 \cdot 10^{11}$	∞
Upper Mantle 1	30	3438	$0.704 \cdot 10^{11}$	3D
Upper Mantle 2	420	3871	$1.055 \cdot 10^{11}$	Case specific
Lower Mantle 1	670	4978	$2.283 \cdot 10^{11}$	$2 \cdot 10^{21}$
Lower Mantle 2	1171	4978	$2.283 \cdot 10^{11}$	$2 \cdot 10^{21}$
Core	2911	10750	0	0

Table 2. Earth model used for the 3D GIA model.

2.3 Temperature models of the upper mantle

For this study two new temperature models are used. Both models are created using LitMod (Afonso et al., 2008; Fullea et al., 2009) which is a modelling framework that links thermochemical conditions in the Earth to geophysical-petrological observations. The rock composition is defined using the major oxide system CFMAS (CaO, FeO, MgO, Al_2O_3, SiO_2). These oxides represent 98% of the mantle material (McDonough & Sun, 1995) and form five independent variables, which are combined in the four main mantle mineral phases (olivine, pyroxene, plagioclase, spinel). Stable mineral assemblages are determined using Gibbs free energy minimization. Heat transfer in the lithosphere is assumed to be by heat conduction; below the lithosphere the temperature follows the mantle adiabat with a potential temperature of 1345 °C (Fullea et al., 2009). For a certain composition, LitMod computes the density and elastic modulus. Different observations can be used to constrain the composition, with the most important being topography and gravity data as explained in the following.

The first temperature estimate used in this study was developed by Pappa et al. (2019) by combining data from topography, seismology and satellite gravity in a lithospheric model of Antarctica in the framework of ESA-project GOCE+. The resulting temperature model for the lithosphere and sub-lithospheric upper mantle is referred to as the GOCE+ model in the following. The crust of the GOCE+ model is divided in a continental and an ocean domain. The continental crust is vertically divided into three layers, representing upper, middle, and lower crust. According to the geological provinces of Antarctica and their estimated tectonothermal age, domains of the lithospheric mantle are defined and described by different peridotitic rock compositions. Using seismologically derived models of the Moho (An et al., 2015a) and the lithosphere-asthenosphere boundary (LAB) (An et al., 2015b) as a starting model, Pappa et al. (2019) modified the Moho and LAB depths in order to achieve a fit of isostasy (topography) and gravity gradients. Since the rock densities inside this model are modelled thermodynamically and internally consistently, a 3D temperature field of the Antarctic lithosphere is a result of that study. The temperature profile of the GOCE+ model for the ASE can be seen in the top row of Figure 3. Compared to the seismically derived temperature profile of An et al. (2015b), temperatures are generally lower.

The second temperature model is the WINTERC 3.2 model (Fullea et al., 2018). LitMod is used here as inversion approach where a variety of geophysical parameters are simultaneously fit to many observations. Isostasy is applied, as well as heat flow data, topography, surface-wave dispersion curves analysis (Schaeffer & Lebedev, 2013) as input. The fit is performed by changing the composition (notably the aluminum content of the lithosphere), the temperature and pressure within the lithosphere model. Temperature maps for the ASE and surrounding regions can be seen in the bottom row of Figure 3.

It can be seen that the GOCE+ model is colder than WINTERC 3.2 model. This is in agreement with the comparison between An et al. (2015b) and the GOCE+ temperature estimates in Pappa et al. (2019). This will result in the GOCE+ model having a higher viscosity than the WINTERC 3.2 model with the same rheology parameters, making it less responsive to short term ice loads. We also see local differences in the spatial pattern between both models. At 70 km a colder region is seen in the GOCE+ model, with warmer parts in the top part of the mantle to the east and west of the ASE. In the deeper layers of the GOCE+ model there is still a colder area north of the coast (110W°) but it is much less pronounced. In contrast, the WINTERC 3.2 model is less uniform in the top layer and has a warmer mantle underneath the ASE, near the northern coast and to the west of the ASE. This translates to a

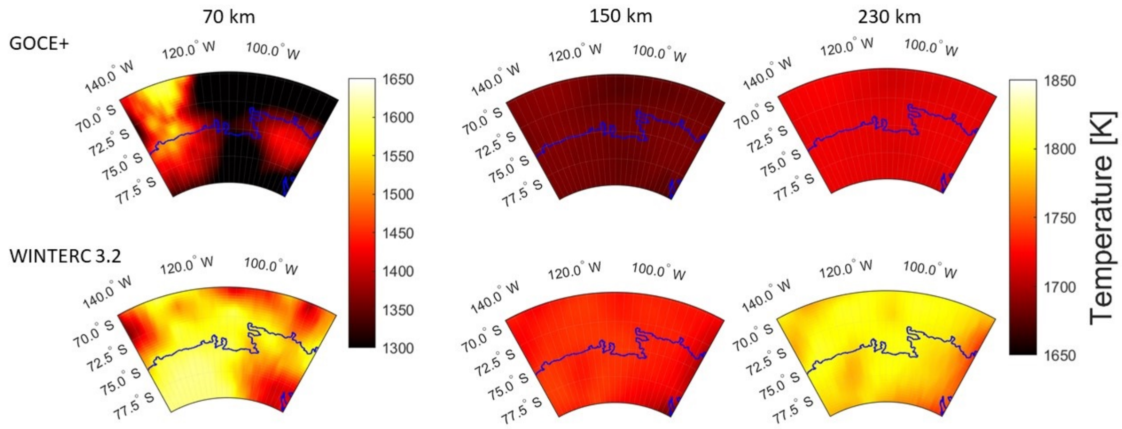

Figure 3. Temperature at 70 km, 150 km and 230 km depth for the GOCE+ model (top) and WINTERC 3.2 model (bottom) for the Amundsen sea embayment (ASE) and surrounding regions.

thinner elastic lithosphere in these locations. In the deeper layers of the WINTERC 3.2 model temperatures are more uniform with the most important differences a slightly colder area to the west of the ASE and also a colder part area in the eastern direction towards the Antarctic Peninsula. Seismic studies, for example Shen et al. (2020), predict low seismic velocities and thus high temperature directly beneath the glaciers of the ASE, showing similarities with the WINTERC 3.2 model.

It is important to note that while there is focus on the ASE itself we use these models to construct a lateral heterogeneous viscosity map for the entire content of Antarctica. This is done because uplift can be sensitive to viscosity in a large area, and because the simulation of the last glacial cycle was done for the entire continent.

2.4 Ice history model

The ice history is derived from the one proposed for the ASE in Barletta et al. (2018). In there, high resolution present-day ice changes during the time period 2002-2014 are extrapolated backwards in time until 1900 (Figure 4). The extrapolated ice loss trend is an overestimation of the actual trend as ice change measurements since the 1970's conclude that ice loss has been speeding up in recent years (Mouginot et al., 2014). At the start of the simulation it is assumed that the load present in 1900 will have been unaltered for 30ky to establish isostatic equilibrium. This is an important difference when compared to Powell et al. (2020) on the ASE, where no loading is applied prior to recent increased ice mass loss. In Barletta et al. (2018) a grid search for the rheology settings for multiple ice history scenarios is performed to find the best fit to the observed GPS uplift. It is found that the ice history scenario which uses 25% of the current trend for the period between 1900-2002, yields the best fit. Because the ice history and the local GIA model used in Barletta et al. (2018) are of a higher resolution than the global FE model used in this study, the ice history is down-sampled from ± 1km to the size of the FE elements discussed in the method section. This down-sampling is also done for the 1D model input to eliminate possible differences as a consequence of different spatial resolution. The ice load that is used as input for the model can be seen in Figure 4.

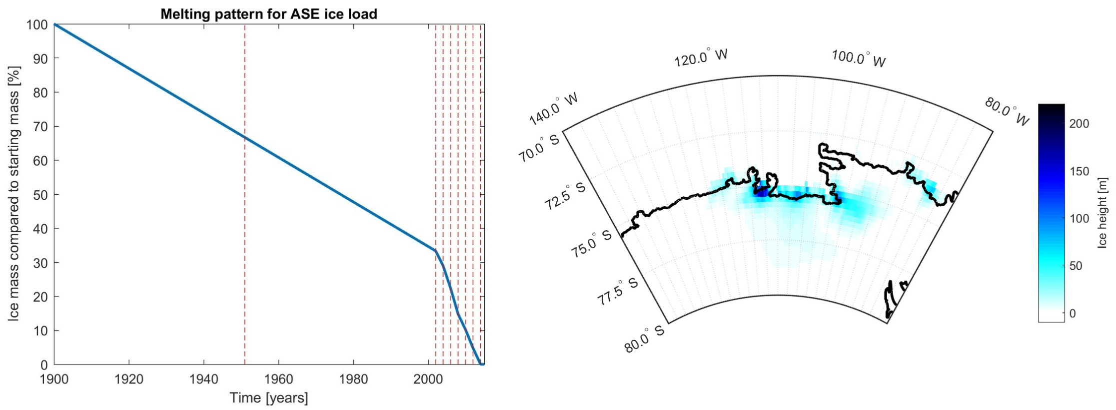

Figure 4. Ice model with the total mass change through time on the left and the spatial distribution on the right.

2.5 The 1D normal mode model

To evaluate the effect of 3D viscosity, the 3D model output is assumed to represent the reality, to which a 1D model is fitted. Here we use the viscoelastic uplift component for a 1D compressible Maxwell Earth model, in response to the ice-mass loss, as in Barletta et al. (2018). The model is based on the normal mode viscoelastic theory where we use the VE-CL0V3RS v3.6 model to compute the elementary viscoelastic time-dependent Green's functions (convolved with Heaviside function) up to degree 1500, and assume that at higher degrees they do not change with time so the combined Green's function is negligible. The structure of the elastic parameter is PREM-based (Dziewonski & Anderson, 1981) with 31 layers, while the viscous parameters are divided into five parts. The first layer is the elastic lithosphere, which is varied in thickness from 40 km up to 70 km and represents the crust and the part of the lithosphere that behaves elastically on the timescale of loading. The second layer is the shallow upper mantle (SUM), which is defined from the bottom of the elastic layer to a depth of 200 km. The third layer is the deeper upper mantle (DUM), which is defined from 200 km to 400 km depth. Viscosities in the SUM and DUM will be varied to achieve a good fit with respect to the uplift from the

3D and 4D models. The final two layers are the transition zone and the lower mantle, which are defined from 400 km to 670 km and 670 km to 2891 km (core-mantle boundary), respectively. These layers have a viscosity of $10^{21} Pa \cdot s$ in this study.

2.6 GPS data

For the GPS stations we have selected the same 6 GPS stations as were used in Barletta et al. (2018) with the addition of the SDLY station (Liu et al., 2018). The SDLY station is located at 125.9746°W, 77.1353°S in Mary Bird land, adjacent to the ASE sector. It was included to also have information on the western side of the ASE. The GPS uplift and their standard deviation can be seen in Table 3.

Stations	Uplift [mm/y]
BACK	10.07 ± 1.5
BERP	19.12 ± 0.7
INMN	26.05 ± 2.4
LPLY	3.93 ± 0.5
THUR	-3.99 ± 0.8
TOMO	29.90 ± 3.0
SDLY	-3.83 ± 1.04

Table 3. GIA associated vertical uplift (Barletta et al., 2018; Liu et al., 2018) of GPS stations in or near the Amundsen Sea Embayment (ASE).

2.7 Statistical model comparison

In order to compare all models evaluated in this study we use a χ^2-test with the χ statistic that is also used in Barletta et al. (2018):

$$\chi^2 = \frac{1}{N_{GPS} - 1} \sum_{i=1}^{N_{GPS}} \left(\frac{\boldsymbol{M_i} - m_i}{SD_{av}} \right)^2 \tag{16}$$

Because both 1D models and 3D models provide exact results and thus no error estimate, we have assumed the standard deviation SD_{av} as the average standard deviation (1.42) of all the real GPS-stations. We use the average instead of the individual standard deviation to avoid introducing a weighting bias to the stations. While the magnitude of this value might be debated, it does not change the ranking of the goodness of fit for models with respect to each other.

In equation 16 $\boldsymbol{M_i}$ is the uplift at the ith-station of the reference model, while m_i represents the 1D model uplift at the same station.

3 Results

We start by exploring which set of rheology parameters of the 4D model best fits the GPS uplift in the ASE. The uplift of this best fitting model will be considered as reality, and it will be investigated how well a best fitting 1D model will approximate the average 3D/4D viscosity. Then, we will investigate whether 3D viscosity results in significantly different uplift rates. Additionally we will inquire if the results are affected by the placement of GPS stations, thus making an assessment of the robustness of any previous findings. After this, we will investigate the effect of time-varying viscosity, by comparing 3D models to a 4D model. Finally, we will test whether including background stress will impact our previous results significantly.

3.1 1D versus 3D/4D models viscosity

To determine which rheology settings would fit the ASE case, we used five sets of grain sizes and water content for the GOCE+ model and four for the WINTERC 3.2 model. The amount of models we can test is limited by the computational resources required. Therefore we performed a limited grid search of the best model by varying the grain size and water content. Grain size is varied from 4 to 8 mm, close to values that give a reasonable fit to uplift in the northern hemisphere (van der Wal et al., 2013). Water content is varied from fully dry to fully wet (1000 ppm water content). Smaller grain size and larger water content both act to decrease viscosity. For both models we have chosen the rheologic parameters for which the chi-squared between the model results and the GPS data was minimal. Including horizontal movement to determine the best fit did not change the best fitting model. The rest of this paper uses vertical uplift only. Using Equation 16 we can compute the χ^2 statistic for every model we considered. The results can be seen in Table 4.

Table 4. χ^2 test statistics per model setting

Grain size [mm]	Water content [H_2O ppm]	GOCE+ model χ^2	WINTERC model χ^2
8	1000	62.4	30.3
6	1000	25.9	222.6
4	1000	10.7	710.8
4	500	10.2	231.8
4	0	109.8	-

Based on the results in Table 4, we selected two models to focus on in this study, with a third model based on one of these first two models. The first model uses the GOCE+ temperature with a grain size of 4 mm and a water content of 500 ppm, which will be referred as G405. The second model uses the WINTERC 3.2 temperature model with a grain size of 8 mm and a water content of 1000 ppm, hence-forth referred to as W810. Two temperature models are used to differentiate between temperature model effects and general effects. Finally, a third model is used, which has the W810 settings for the rheology but dislocation creep is ignored by forcing the Von Mises stress to 0 using equation 12. This is done in order to eliminate the time-variance of viscosity. Using a Von Mises stress of 0 will lead to an overestimation of viscosity. However, it is impossible to find a single accurate representative average Von Mises stress. The resulting model is a 3D model instead of a 4D model and will be referred to as W810-3D.

In Figure 5, the effective local viscosity is shown for G405 and W810 at two different points in time, approximately halfway through the deglaciation, in 1951, and at the end of the simulation in 2014. W810-3D is time-invariant and is shown in the bottom row. The viscosity highly correlates with the temperature map (Figure 3) for all models, with the only deviation present in high stress areas near the ice load. The G405 model shows high values for the viscosity at 70 km depth with the exception of the western-most region. As the depth increases, the viscosity drops and becomes relatively uniform in horizontal directions. Changes in viscosity over time are small for G405. For W810, at 70 km, there is a significant difference between the viscosities in the east and west of the ASE. In the centre of the ASE, there is an area of very low viscosity ($10^{18.0} Pa \cdot$ s) at 2014; this is where the glaciers are located with the largest mass discharge (Thwaites). This local low viscosity area is caused by the stress which is induced by the change in ice load. As the simulation approaches present day, the changes in ice load are larger than a few decades earlier. This increases the maximum stress from around 170 KPa in 1951 to more than 0.5 MPa in 2014 for the final time step. The high local stresses cause dislocation creep to become a more dominant creep mechanism over a larger area which lowers the local viscosity over this area significantly. The load induced stress is reduced with increasing depth and therefore the change in viscosity over time is larger at 150 km than at 230 km. The last model, W810-3D, has the same east-west viscosity differences in the top part of the mantle as we observed in the W810 model. In both the W810 and the W810-3D model there is an area in the east of the ASE (95°W) that has a higher viscosity compared to the neighbouring coastal regions. The deeper parts of the mantle are more uniform with slightly higher viscosities towards the east in the direction of the Antarctic rift system.

To see how well the best-fitting 1D model represents the 3D structure, a representative 1D viscosity and elastic thickness of the 3D and 4D models has to be determined. It is not ob-

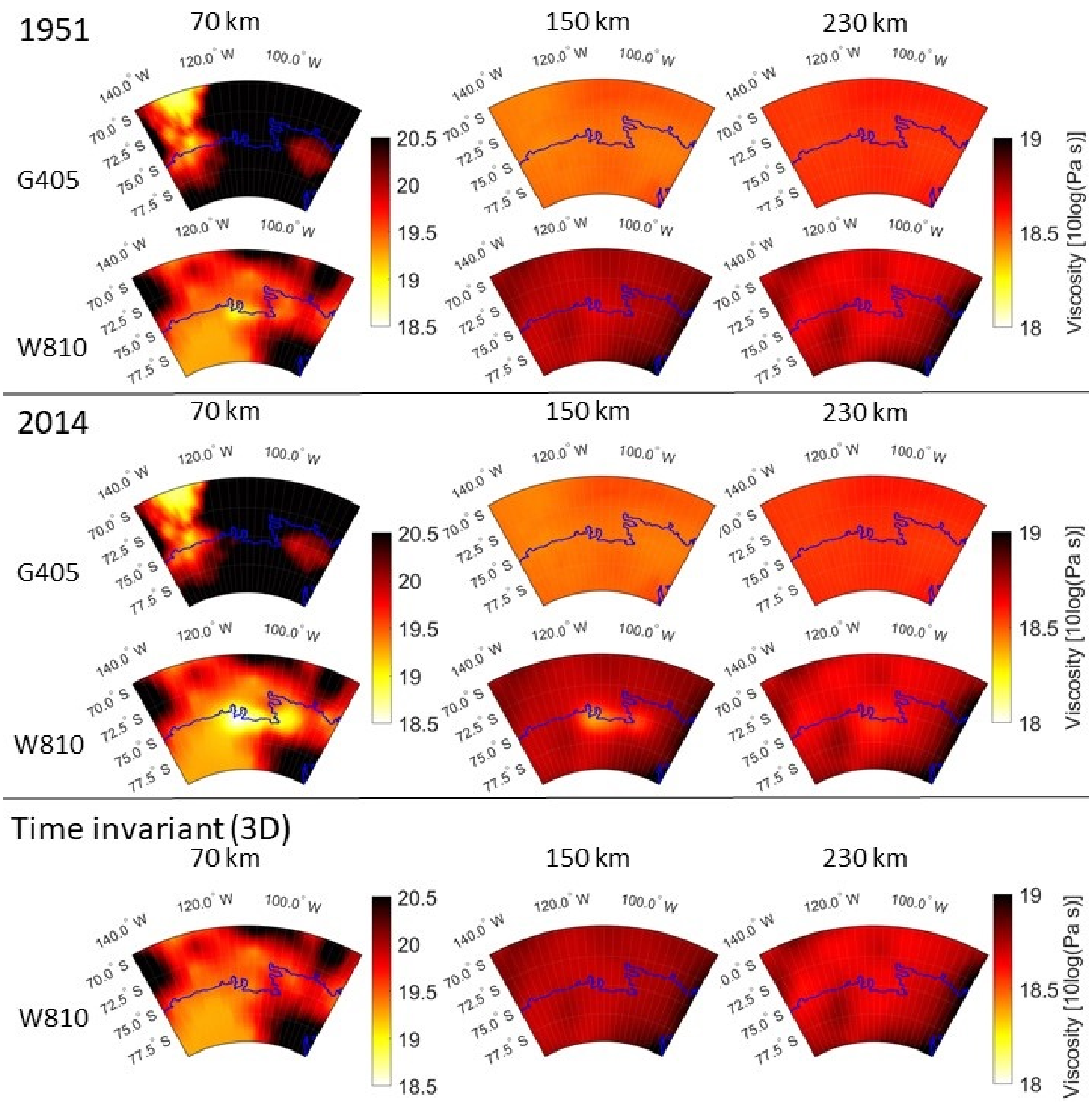

Figure 5. Viscosity of the ASE for three different depths: 70 km, 150 km and 230 km. The models displayed are G405, W810 and W810-3D. The top two rows show the viscosity in 1951, which is near the halfway point of the simulation. Rows 3 and 4 shows viscosities in 2014, which is the last epoch in the simulation. The bottom row shows the viscosities for the W810 version with stress independent rheology.

vious how such an average should be computed from a 3D/4D model with a local load. The first step is determining which elements behave viscoelastic and which elements are almost exclusively elastic. Although the thickness of the purely elastic layer is 30 km in the 4D model the effective elastic lithosphere thickness can be larger. In order to estimate the viscosity for which we would consider an element elastic we consider the relation between Maxwell viscosity and relaxation time:

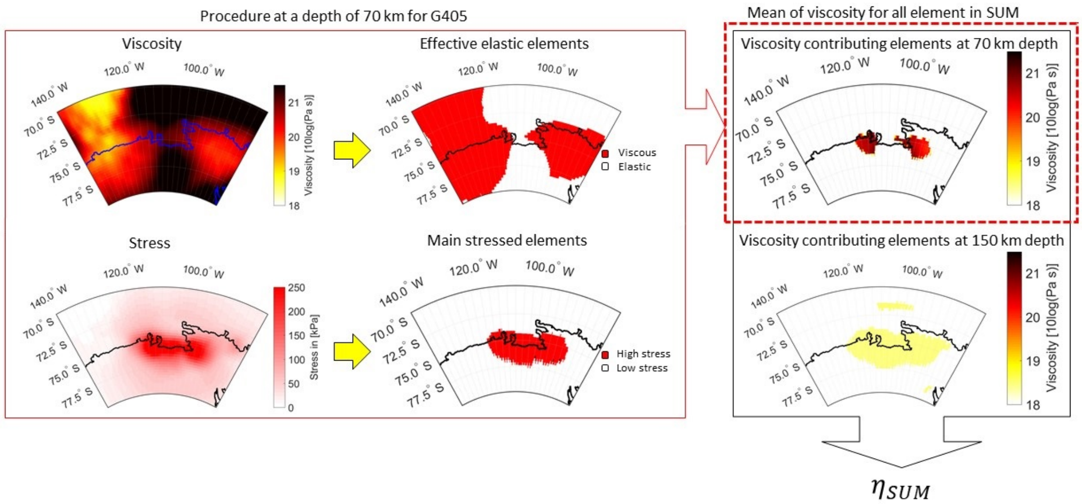

Figure 6. Schematic overview of the procedure to compute an average viscosity based on stress for the SUM of the G405 model. The starting values are the viscosity and the stress at any given depth (70 km in this example). The viscosity is used to determine which elements show viscous behaviour (red) over the course of the simulation (η<21.0 $\log_{10}$(Pa · s)). A stress threshold is used to determine the elements that contribute significantly to the uplift (red). If an element is both viscous and high-stress its viscosity is used to compute η_{SUM} together with elements that also fulfil these conditions.

$$\eta = \tau G \tag{17}$$

As a threshold for an elastic element, 3 times a relaxation time of a 150 years of simulation is assumed. With the shear modulus G as stated in Section 2. We find a threshold value of $10^{21.0} Pa \cdot s$. By assuming elements of a viscosity larger than $10^{21.0} Pa \cdot s$ to be elastic we can derive an average elastic lithosphere thickness D_{litho} using relevant elements for GIA. The contributing elements are selected based on a threshold Von Mises stress, relative to the highest Von Mises stress at the depth at which the element is located. For the elastic elements we did not consider elements deeper than the SUM. We compute the fraction of elements within a selection that have a viscosity higher than $10^{21.0} Pa \cdot s$, $\frac{N_{\eta>21_i}}{N_{total_i}}$, and multiply this with the layer thickness D_i. Finally, the thickness of purely elastic layer, D_{crust} is added (Equation 18) and the results are shown in Table 5. We can see in Table 5 that G405 has a larger elastic lithosphere (53 km), while the elastic lithosphere thickness for the W810 and the W810-3D model is consistently 30 km.

$$D_{litho} = D_{crust} + \sum_{i=1}^{n_{layers}} D_i \frac{N_{\eta>21_i}}{N_{total_i}} \tag{18}$$

When we have defined which elements can be considered elastic we exclude them from the viscosity averaging computations. The average viscosity for the SUM and DUM is estimated by selecting the contributing elements based on a threshold Von Mises stress, relative to the highest Von Mises stress at the depth at which an element is located. An unweighted average is taken for the selected elements in this method. An overview of the method can be seen in figure 6. It can now be investigated whether the best fit 1D model viscosities are close to the average viscosity values of the FE model (Table 5).

3D/4D model	Layer parameter	Time [AD]	G405	W810	W810-3D
Averaged Values of contributing elements	D_{litho} [km]	1951	59.8	30.0	30.0
		2014	53.2	30.0	30.0
	η_{SUM} $[log_{10}(Pa \cdot s)]$	1951	18.94	19.22	19.08
		2014	18.91	19.02	19.08
	η_{DUM} $[log_{10}(Pa \cdot s)]$	2014	18.66	18.88	18.89
Best fitting 1D models	Layer parameter		G405	W810	W810-3D
N = 7	D_{litho} [km]		70	40	50
	η_{SUM} $[log_{10}(Pa{\cdot}s)]$		19.2	18.4	19.0
	η_{DUM} $[log_{10}(Pa{\cdot}s)]$		18.4	18.8	18.8
N = 1440	D_{litho} [km]		70	40	60
	η_{SUM} $[log_{10}(Pa{\cdot}s)]$		19.2	18.6	19.0
	η_{DUM} $[log_{10}(Pa{\cdot}s)]$		18.4	18.8	18.8

Table 5. Top section: Average elastic thickness (D_{litho}) and viscosity for the shallow upper mantle layer (η_{SUM}) and the deeper upper mantle layer (η_{DUM}) of the 3D and 4D models using stress based selection of the elements. The SUM values are shown for both 1951 and 2014, while the DUM values are only shown for 2014 as there is little variation in this layer over time. Bottom section: Elastic thickness and viscosity for the SUM and DUM of the best fitting 1D model with respect to each of the 3D/4D models using the 7 GPS sites (N=7) a grid of points [71.25°S,80°S; 80.625°E,130°E] (N=2880)

.

To benchmark how reliable the comparison is between the 1D and 3D/4D viscosity, a homogeneous 4D model was run with a crustal layer of 40 km and non-linear rheology parameters that should correspond to an effective viscosity of 19.0 $\log_{10}(\mathrm{Pa} \cdot \mathrm{s})$ for both the SUM and DUM. The best fit 1D model for this case was a model with a 40 km effective elastic lithosphere, a η_{SUM} of 18.8 $\log_{10}(\mathrm{Pa} \cdot \mathrm{s})$ and a η_{DUM} of 19.0 $\log_{10}(\mathrm{Pa} \cdot \mathrm{s})$. While very close to the parameters of the 4D model, small differences between 1D and 3D/4D are introduced because of difference in discretization.

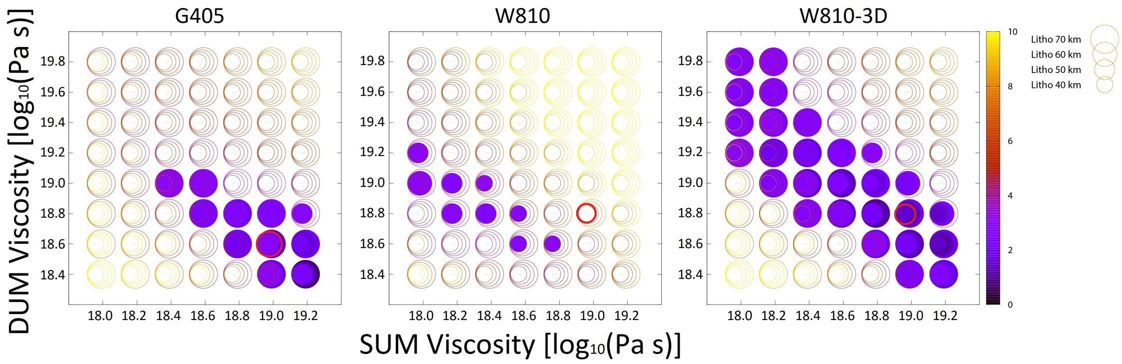

Figure 7. χ^2 of the 1D models with respect to simulated uplift of 3D/4D models as a function of viscosity in the shallow upper mantle (SUM) and the deep upper mantle (DUM). Every circle is a single 1D model, with the color indicating the χ^2. The circle size denotes models with different lithospheric thickness. All solid circles represent models that fall within the 95% confidence interval. The red circle represents the average viscosity for the 3D/4D model.

In Figure 7, it can be observed that there are multiple models with a good fit (95% confidence interval, which equals $\chi^2 < 9.49$ or $\chi < 3.08$). The best fit 1D models in this paper for model G405 and W810-3D have a better fit to these 3D/4D models than to the GPS uplift rates, as was computed in Barletta et al. (2018) while model W810 has a similar value. Taking into account that for this experiment the ice history is perfectly known it can be concluded that G405 and W810-3D will be indistinguishable from a 1D model given the worse fit of any model to the uplift using 7 stations in reality. More GPS stations or input stations with a lower standard deviations in the data would be needed to discriminate the 3D effect from the 1D effect.

We now investigate whether the 1D viscosity obtained from the fit is close to the average 3D viscosity. In table 5 we see that for all three models the viscosity for the DUM is estimated to be slightly lower (maximum of 0.3 $\log_{10}(\mathrm{Pa \cdot s})$) than the average computed from the 3D/4D models. For both the G405 and the W810-3D models the difference between the 1D and 3D/4D models in SUM viscosity is (0.29 $\log_{10}(\mathrm{Pa \cdot s})$ and 0.08 $\log_{10}(\mathrm{Pa \cdot s})$). For the W810 model the SUM viscosity in the 1D model underestimates the average 3D viscosity. This means that for the W810 model both the SUM and DUM 1D estimated viscosities are lower than the average viscosity. This suggests that the uplift is determined to a larger extent by a small region of low viscosity, which is not reflected in the average viscosity. The misfit of the 1D model does not strongly depend on elastic lithosphere thickness, which becomes evident from the W810-3D case. Here the 1D model prefers a thicker lithosphere but the viscosity is still the closest possible estimate. The inversion tends to prefer thicker elastic lithosphere values for the G405. In Barletta et al. (2018) it was suggested that there could be a trade-off between upper mantle viscosity and elastic lithosphere thickness, which we see for the G405 model.

We investigate whether having limited GPS data will change the best fit 1D model with respect to the 3D/4D models. The best fitting model in terms of uplift is determined using 1440 reference points (all coinciding grid-points between the models) instead of only the 7 original GPS locations (Table 5). For the G405 case there is no effect of placing more stations, as 7 stations will result in the same best fit as with 1440 stations. While this is not true for the W810 and W810-3D cases, we can still note that in these cases, the current 7 stations also give best fit models that have small differences in lithosphere thickness (10km) or η_{SUM} (0.2 For the SUM) with respect to the best fit models with a large amount of stations. This leads us to conclude that the current 7 stations already form an adequate data set to perform reliant inversions when determining a representative 1D viscosity.

The resolution of the FE model is fixed to the values in Table 1 and Figure 1 to limit the computation time, and interpolation is required at multiple stages, for example from the ice history data to loads applied to the finite elements or to find uplift and locations in between model nodes. To investigate the impact of this issue we have compared GPS station uplift not only on their exact locations but also on the closest model nodes. Altering the GPS locations has a small effect on the chi-squared values of the best fit, but not enough to change the best fitting models in this paper. Changing interpolation methods for the computation of the gravitational perturbation changes the average uplift by approximately 0.2%. Changing the vertical resolution can have a stronger effect on the results, because the changes in temperature in radial direction are larger than the those in lateral direction. However, GIA models can not invert uniquely for many layers, and our results are valid for the layering in the upper mantle selected for the 1D model.

3.2 1D versus 3D/4D models uplift

To investigate whether 1D models can represent the uplift pattern of a 3D or 4D model, Figure 8 shows the difference in uplift between the 3D/4D models and their respective best fitting 1D model. In general we can see that it is not possible for the best fit 1D models to fit any of the 3D models everywhere even though the models do not differ in a statistically significant fashion. This is because for most GPS locations the best fit 1D model uplift is close to the 3D/4D models uplift, although for every model there are 1 or 2 GPS stations that have a local bad fit (more than 2 σ difference). Locations in between the GPS sites can still show large differences (23.1 mm/y difference for W810 and 6.7 mm/y difference for W810-3D). The GIA uplift pattern, for the W810 and W810-3D model, has a sharper peak with a higher uplift than the best fitting 1D model at the point of maximum unloading (cross-section **a**). At cross-section **b** this is the same for W810 and reversed for W810-3D. At 76°S in cross-section **a** we see more local uplift for W810 and W810-3D than the 1D model as a because of low local viscosity, either as consequence of the high lithosphere temperature by itself or in combination with high local stress. The different patterns in the cross-sections show that it is not possible for a 1D model to fit the uplift pattern of the 3D/4D model everywhere, as a change in viscosity does not only change the magnitude of the uplift but also the spatial distribution of the uplift.

We showed earlier that more stations does little to change the best 1D model for each of the 3D/4D models, and that with the current data the 1D models can not statistically be distinguished from the 3D/4D models. However, Figure 7 illustrates that this does not mean large differences do not exist and that with more GPS stations in the right locations 3D/4D differences could be detected. Having a GPS station in between the BERP and TOMO station (120°S 76°W) would give the best indication on possible low local viscosity. Another location that might give insight in the 3D effect is around 75.5°S 95°W in Ellsworth Land. This area gives large differences as a consequence of a high viscosity area. It must be noted that this high viscosity area is present because of the low temperature area in the WINTERC model; in the GOCE+ model this area has a higher temperature which would result in a lower viscosity.

3.3 Effect of time-varying viscosity

In this section we investigate whether 4D rheology gives significantly different uplift compared to 3D rheology, and if any 3D rheology can approximate the effect of 4D rheology. We use model W810 with varying stress, and compare it against W810 models in which stress is set to a constant level. Ideally, we would choose the Von Mises stress such that the time-averaged effective viscosity is the same, or the uplift differences are minimized as is done with the 1D model inversion. However, this is computationally expensive. Instead we use a low stress (0 kPa) and a high stress (300 kPa) as lower and upper bound, respectively. This results in a respectively significantly higher and lower average viscosity than computed in Table 5. We scale these uplift patterns to minimize the difference in maximum and minimum occurring uplift. The idea is that the pattern in uplift is largely fixed, but the magnitude will be changed as a function of Von Mises stress, which we reproduce by scaling the uplift. To support this idea we confirmed that upscaled results and downscaled results give a similar result (Figure 9 right column).

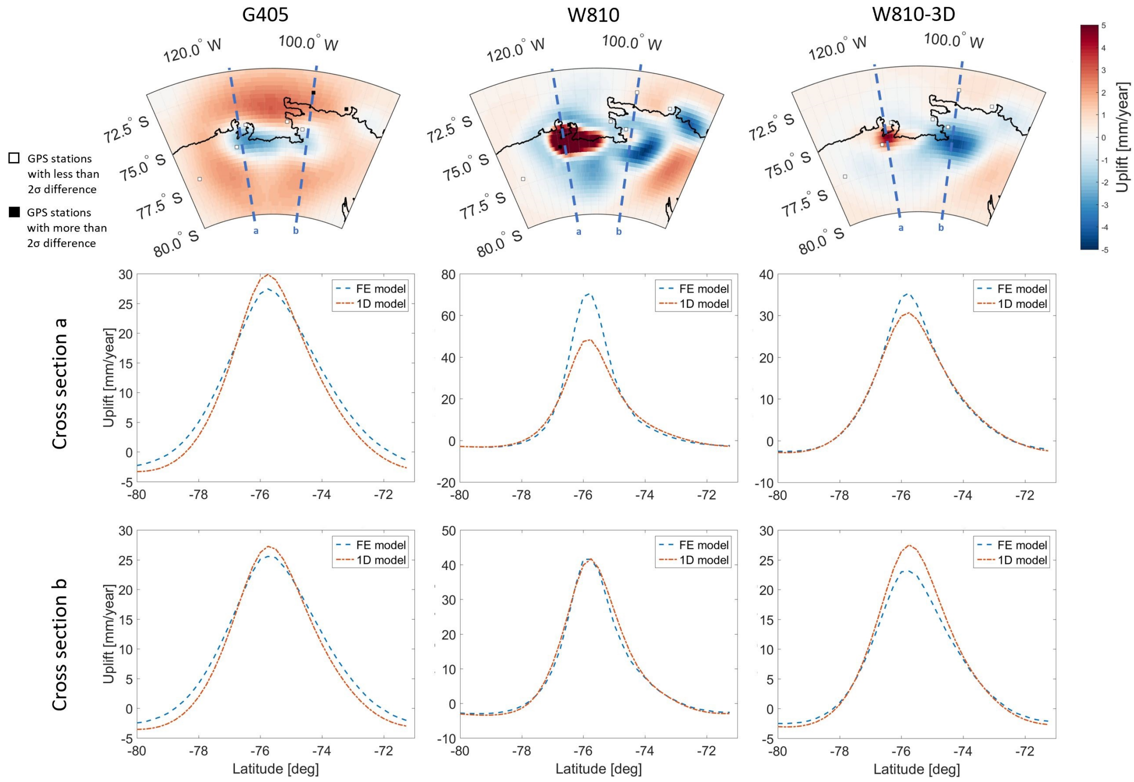

Figure 8. Top: uplift of the three models minus their best fitting 1D model. The black squares are GPS stations where the differences exceed 2σ (95% confidence), the white squares are stations where the differences are below 2 σ. Center: cross section of the uplift of all three models and their best fitting 1D model at the 113.75W° meridian (**a**), which intersects the point of maximum uplift. Bottom: cross section of the uplift of all three models and their best fitting model at the 97.5W° meridian (**b**), where the differences between the three models and their best fitting 1D model are the largest.

In Figure 9 we observe that the model without stress underestimates the uplift due to the higher viscosity, while the model with 300 kPa constant stress overestimates the uplift due to the lower viscosity. The differences after scaling are positive in the center of loading and negative outside. This is the result of the constant stress models having a more spread-out uplift pattern than the 4D model. The average differences can not be reduced further by scaling the uplift and when computing the the χ^2 statistics for the scaled 3D models at the location of the GPS stations we obtain values of 0.23 and 0.15, respectively for the 0 KPa scaled result and the 300 KPa scaled result, which could be considered close fits. However, the 3D model still shows up to 14 % less uplift at the point of maximum uplift. The higher uplift in the 4D model can be traced back to the viscosity decrease under the load, as stress increases (see Figure 5). It must be noted that in Figure 8, the G405 model did not show more localized uplift despite it being a 4D model. That is because the G405 model was created using a smaller grain size

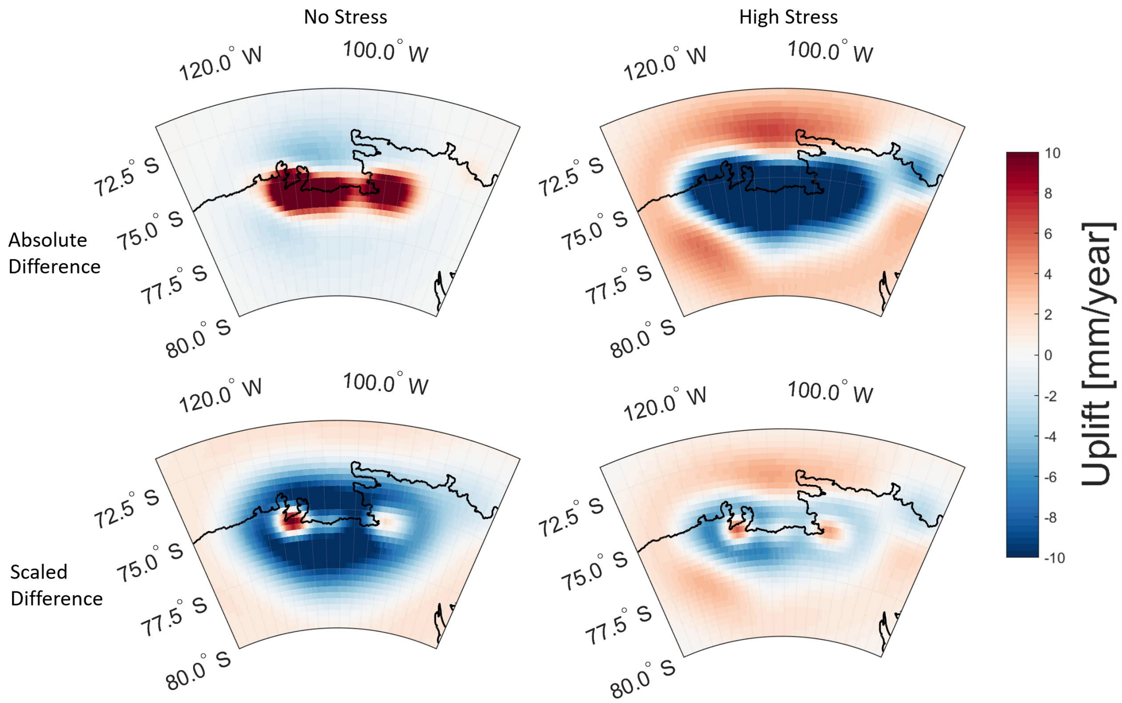

Figure 9. Differences in uplift: W810 a stress dependent viscosity minus W810 with a constant stress (and hence constant viscosity). Left column: Difference between W810 and W810 without stress (W810-3D) induced viscosity changes. Right column: Difference between W810 and W810 where a constant Von Mises stress of 300 KPa is applied. Top row: the absolute difference between aforementioned models. Bottom row: The difference when the constant stress models are scaled to minimize the differences differences, with a factor 1.73 and 0.73, for the 0 kPa case and the 300 kPa case, respectively.

and a lower water content, which results in a lower contribution of dislocation creep (Kohlstedt, 2007; Barnhoorn et al., 2011). In conclusion, a 3D model can not reproduce the uplift from a 4D model completely.

Nield et al. (2018) found similar differences between 1D models and models with non-linear rheology in the Antarctic Peninsula noting the more localized uplift in the latter, as represented by differences in gradients in uplift. An important caveat is that no background stresses are included. The addition of long-term GIA stresses is investigated in section 3.4 but the interaction with stresses from other processes such as mantle convection and post-seismic deformation is left to future work.

3.4 Effect of background stress

In all previous evaluations we only included the effects of a recent ice history as described in Section 2.4. However, as can be seen in Equation 14 for non-linear rheology viscosity is a function of total stress. Processes such as mantle convection, post-seismic deformation, and stresses from earlier ice loads could contribute to the total stress in the mantle and could change the effective viscosity. Larger stress will increase the contribution of dislocation creep, but at the same time it might decreases the relative importance of stress changes over time due to the loading. As stated in section 2.2, adding a background stress can either increase or decrease the change in viscosity over time due to load induced stress changes, depending on the ratio of diffusion to dislocation creep parameter. Figure 2 shows us that for a ratio of around 15 orders of magnitude between diffusion and dislocation creep parameters a small load will cause a larger reduction in viscosity than a larger load. In the G405 model the ratio between diffusion and dislocation for upper mantle elements in the ASE is between 13 and 14.5, which falls in the aforementioned window where there is a larger reduction in viscosity when loads are added with a background stress present compared to the same load case without background stress. For a wet model, such as W810, this effect is less of a issue as the ratio between diffusion and dislocation is limited between 12 and 13.5 and thus the majority of the time the reduction in viscosity is less when the load is added with a background stress compared to case without background stress. The influence of a homogeneous background stress can be seen in figure 10, where we look at the change in viscosity as a consequence of load induced stress. The left column in figure 10 is close to the viscosity change we can see in Figure 5 between 1951 and 2014. For the right column in Figure 10 a background stress of 1 Mpa is added to the load induced stress for both the G405 model and the W810 model. Only the change in stress invariant is considered here, similar to Gasperini et al. (1992) and Wu (2001).

The G405 model shows an increase in viscosity change when the background stress is added. Here the increasing background stress increases the importance of dislocation creep relative to diffusion creep which makes the rheology respond stronger to stress changes, as shown in Figure 2. In the wetter W810 model the dislocation mechanism is more pronounced meaning that adding background stress will dampen the viscosity changes as a consequence of time-varying stresses.

Figure 10 is essentially a snap-shot of the present day viscosity if a background stress were to be introduced suddenly, which assumes it to be in the same principle direction as the load stresses and thus the Von Mises stress simply being the sum of both stresses. In reality a background stress field has different components, which means that the Von Mises stresses can not be super-imposed because stresses can cancel each other (Schmeling, 1987). Next we take the latent stresses from GIA as a result of the millennial scale ice load changes that occured since the LGM as a source of background stress. We introduce this stress by running the model a full glacial cycle before the simulation enters the recent ice history as described in Section 2.4.

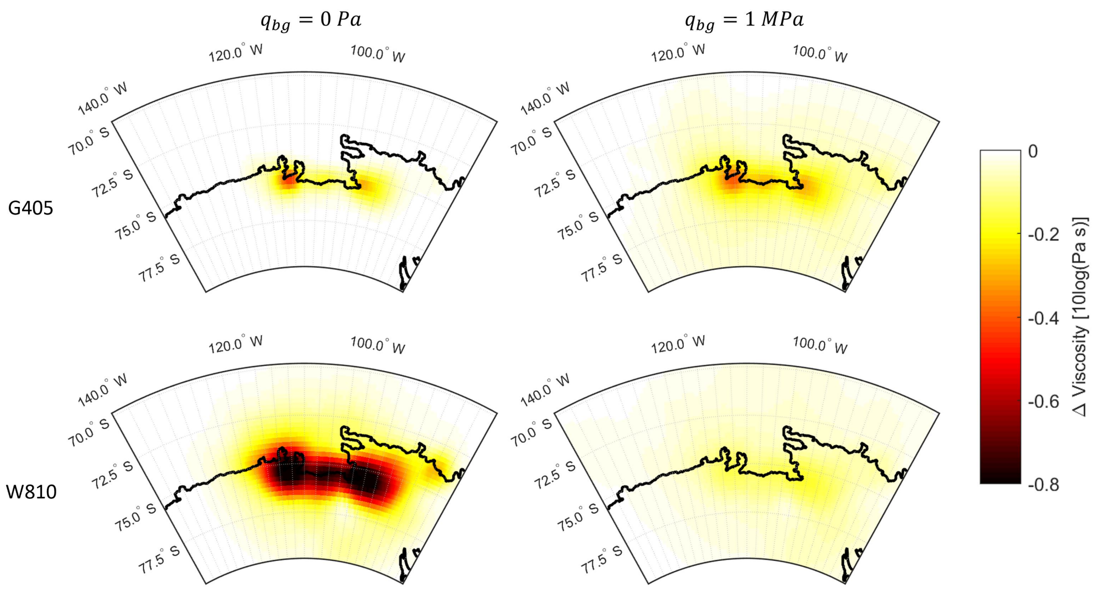

Figure 10. The change in viscosity as a consequence of load induced stress by means of dislocation creep at the end of the ASE simulation. Left: the differences in viscosity when no additional background stress is considered. Right: the differences when a 1 MPa background Von Mises stress is added. Top: both background stress cases for the G405 model. Bottom: both background stress cases for the W810 model.

The full glacial history assumed here is the W12 model (Whitehouse et al., 2012). As a consequence the model will start with stress in the lithosphere which influences the starting viscosity. The change in viscosity as a consequence of the glacial cycle stresses can be seen in Figure 11. As a consequence of the higher viscosity in the G405 model in general more stress from the ice age loads is still present at the start of the simulation, leading to a stronger reduction in viscosity compared to W810. In W810 a larger portion of the stress has dissipated in 1900 leading to a lower viscosity drop overall. This means that while wet models have a decreased viscosity drop with background stress compared to dryer models, they also have a smaller background stress as the ductile mantle allows those models to dissipate the stress more quickly. Both the stress itself as the reduction in viscosity strongly affects the uplift for both the G405 and the W810 case. These uplift results can be seen in Figure 11. We now investigate the effect on the conclusions from section 3.3 by comparing results with and without the inclusion of the W12 ice history (Figure 11). For G405, the uplift when a full glacial history is included, is largely determined by the ice loads from before 1900. For W810 the uplift is very similar in spatial pattern to the uplift obtained from recent ice loads, with the only difference the increase in magnitude. The fact that the G405 is influenced by the loads before 1900 and the W810 is not, is

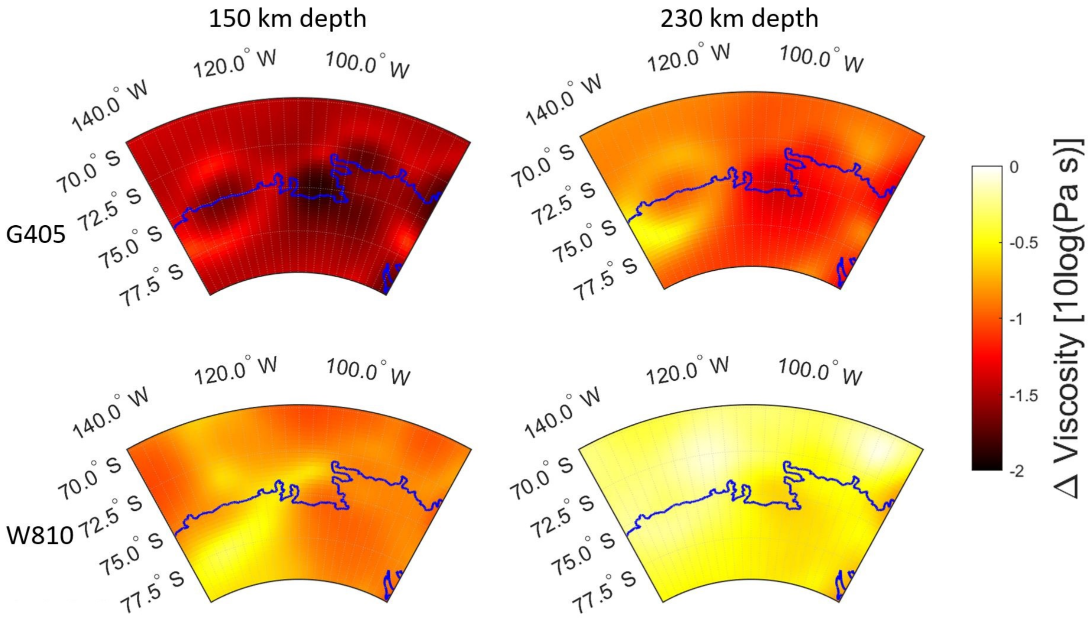

Figure 11. The change in viscosity as a consequence of ice age induced background stress by means of dislocation creep at the start of the ASE simulation. Left: the reduction in viscosity at 150 km depth. Right: the reduction in viscosity at 230 km depth. Top: Viscosity profiles at different depths with background stress present for the G405 model. Bottom: Viscosity profiles at different depths with background stress present for the W810 model.

caused by the high viscosity layer in the G405 model compared to the W810 model. This high viscosity layer is still stressed at the end of the simulation from ice loads predating 1900. However, high viscosity models are unlikely given the good fit Barletta et al. (2018) achieved only considering recent ice changes. In order to understand the effect ice age stress has on current day uplift through changes in viscosity, the non-linear component in the uplift was computed by combining the uplift from recent ice mass changes with the uplift from the ice age simulation (so there is no stress interaction) and subtract those from a single simulation where both ice histories are present (where there is stress interaction). For W810 we see that the pattern of the non-linear component matches both the uplift as a consequence of the current ice mass changes as well as the uplift from the combined ice history. If we scale the results of the combined simulation to match the results that only include recent ice changes, the resulting difference is very low. From this we can conclude that for wet models or models with low viscosity in general, background stress can have a significant effect on the total uplift as a consequence of an overall lowering in viscosity. However, as a significant portion of the background stress dissipates quickly, especially for regions that have high local stress, the overall effect on the spatial uplift pattern is limited. Areas that have experienced recent high load changes will still have

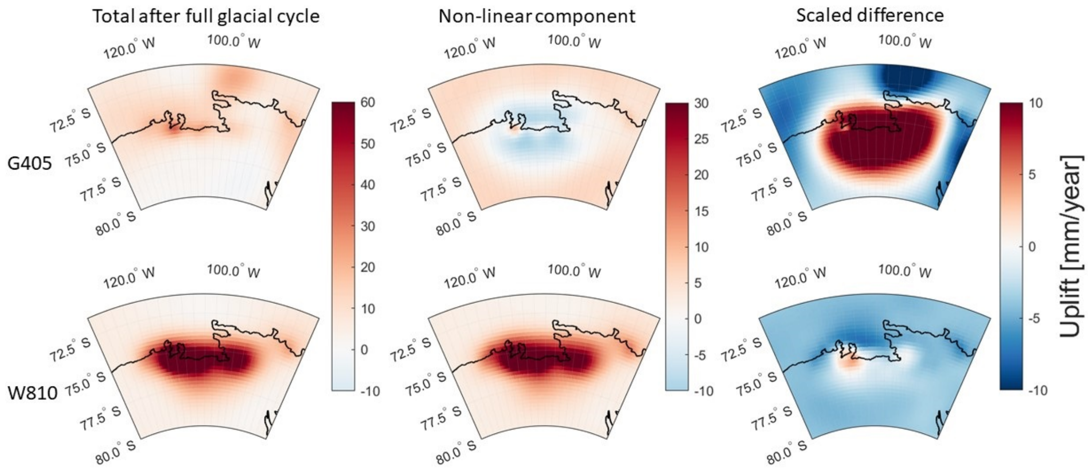

Figure 12. Left: uplift for both the G405 model and the W810 model when loaded with the W12 ice history as well as the recent ice history from Figure 4. Centre: The difference between the uplift of full glaciale cycle with recent loads combined in a single run and the uplift of both of those components in separate runs. This is the uplift as a consequence of the non-linear component in the rheology. Right: the uplift of the models without glacial history are scaled such that the differences squared as shown in the central column are minimized

more localized uplift compared to 3D and 1D models. For G405 the situation is different as the high amount of stress in the mantle present at 1900 both changes the viscosity and local Von Mises stress such that non-linear component does not show a straight forward magnitude change in the uplift, but instead even shows area's where the non-linear component is negative. In these area's background stress and recent ice load stress have cancelled each other to some degree. The conclusion here is that for high viscosity or dryer areas, where one might expect the role of stress over time to be limited considering the small contribution of dislocation creep, non-linear rheology can still have a large impact on the final results. Even though changes in viscosity over short time frames will be less likely for these cases, the high viscosity means that stress will linger for a longer time which increases the chance of stress from different processes or time periods to interact and affect viscosity. As a consequence of the overall lowered viscosity the uplift response at present is stronger.

4 Conclusions

In the ASE region there is evidence for varying mantle structure which manifests as viscosity variations of one order of magnitude. Given the importance of dislocation creep in mantle deformation, it is also possible that stress changes induce viscosity changes over time and space. We simulate uplift with two different 4D models and a 3D model with olivine rheology with varying grain size, water content and spatial variations as a function of temperature and stress. We perform a 1D model inversion for the uplift of these models to find out how close the 1D model predictions are those of the 3D/4D models.

We investigate two different temperature models based on inversion of the petrophysical-geophysical framework LitMod, with one largely based on gravity data (GOCE+) leading to more spatially homogeneous temperature and higher viscosity, and the other relying more on seismic data (WINTERC 3.2), resulting in lower viscosity and more spatial variations. For each temperature model, rheological parameters from a limited range are taken which best fit GPS uplift in the ASE. The first of the three models, G405 is based on the GOCE+ temperature profile, has a small grain size of 4 mm and a rheology between fully wet and dry olivine. The effective viscosity is rather homogeneous and has a small 4D effect. The second model, W810, is based on WINTERC 3.2 and has a large grain size of 8 mm and fully wet rheology. For the latter model stress-dependence can be switched off by prescribing stress to be constant. This model is refered as W810-3D

The first main conclusion is that the best-fitting viscosity in the 1D models is close (difference of $0.3 \log_{10}(\mathrm{Pa} \cdot \mathrm{s})$ maximum) to the average viscosity of the 3D and 4D models in the upper mantle between 200 and 400 km. At this depth the influence of 3D and 4D variations is small. For the viscosity estimate of depths shallower than 200 km the best fitting 1D models also find good viscosity estimates for the models with low to no time-varying viscosity. However, for W810, where stress changes reduce local viscosity more significantly, the 1D viscosity does not represent the wider regional viscosity, but is biased towards local viscosity at present underneath the largest mass changes. In that case deviations to modelled reality can be more than half an order of magnitude. Recent studies demonstrating abnormally low viscosity underneath the ASE likely accurately reflect a weighted average of a current 3D viscosity structure in the region with a stronger influence from the low viscosities under the sites of the largest mass changes.

We found that the differences between 1D and 3D models in uplift is, possibly significant depending on the locations in the ASE and the 3D model assumed. This is in contrast to Powell et al. (2020) where they found little to no significant difference in vertical movement between 1D and 3D models. However, they did not include non-linear rheology, which as shown in this study can increase difference with 1D models significantly. Furthermore, they used a different ice loading setup for their model which reduced the overall uplift of the stations in the ASE both compared to models in this study and real world data, which can further decrease any potential difference between model types. While it is important to note that in that the difference between 1D models and the real world situation might indeed be small, this study shows that there is also a very real possibility that it is not

For 4D models, the stress-dependence of viscosity creates a temporary region of low viscosity below the load. This makes uplift patterns more local for the 4D model compared to the 1D and 3D model. The uplift near the point of maximum stress is underestimated by the best fitting 1D model, while uplift in surrounding areas and the collapse of the forebulge is overestimated; the 1D model can not fit both regions simultaneously. If 1D models are used to correct GIA effect in mass change measurements it could mean that GIA derived gravity rate is too low at the area of maximum mass loss and too large elsewhere. However, this result is sensitive to the magnitude of ice load changes and even more to the presence of background stresses.

When including background stresses, such as a full glacial cycle, the load induced viscosity drop can be amplified or weakened, depending on the relative importance of diffusion and dislocation creep. A dryer model, such a the G405 model falls within the category for-which including background stress increases these viscosity drops. Due to a high viscosity in the upper mantle, G405 showed uplift patterns that were influenced by stress changes due to ice mass changes from before 1900, while the low viscosity upper mantle of the W810 model meant that stresses from earlier deglaciation were already decayed. From Barletta et al. (2018) we know that observed uplift can be modelled to a high degree by only using the recent ice history. This indicates that a low viscosity mantle such as in the W810 or W810-3D model is more likely to be representative of the actual mantle underneath the ASE. However, for both the G405 model as the W810 model the inclusion of stress from the LGM ice loads did change the uplift result significantly, suggesting that background stresses have to be included in areas of large past ice load changes. Stresses due to LGM ice load changes can be similar to or smaller than those of mantle convection. In the presence of large mantle convection induced background stress, the effect of 4D rheology used in this study is even more unpredictable. As the background stress components are uncorrelated with the components of load induced stresses. The effect of mantle induced background stress is an important topic for future study.

4.1 Acknowledgements

This study was funded by NWO under the project ALW.GO.2015.042. The work has been carried out in the course of the project GOCE+ Antarctica funded by ESA as a Support to Science Element.

References

A, G., Wahr, J., & Zhong, S. (2013). Computations of the viscoelastic response of a 3-D compressible Earth to surface loading: an application to Glacial Isostatic Adjustment in Antarctica and Canada. *Geophysical Journal International*, *192*(2), 557-572.

Afonso, J. C., Fernàndez, M., Ranalli, G., Griffin, W. L., & Connolly, J. A. D. (2008). Integrated geophysical-petrological modeling of the lithosphere and sublithospheric upper mantle: Methodology and applications. *Geochemistry, Geophysics, Geosystems*, *9*(5).

An, M., Wiens, D. A., Zhao, Y., Feng, M., Nyblade, A., Kanao, M., ... Lévêque, J.-J. (2015b). Temperature, lithosphere-asthenosphere boundary, and heat flux beneath the Antarctic Plate inferred from seismic velocities. *Journal of Geophysical Research: Solid Earth*, *120*(12), 8720-8742.

An, M., Wiens, D. A., Zhao, Y., Feng, M., Nyblade, A. A., Kanao, M., ... Lévêque, J.-J. (2015a). S-velocity model and inferred Moho topography beneath the Antarctic Plate from Rayleigh waves. *Journal of Geophysical Research: Solid Earth*, *120*(1), 359-383.

Barletta, V., Bevis, M., & Smith, B. (2018). Observed rapid bedrock uplift in Amundsen Sea Embayment promotes ice-sheet stability. *Science*, *360*(6395), 1335-1339.

Barnhoorn, A., van der Wal, W., Vermeersen, B. L. A., & Drury, M. R. (2011). Lateral, radial, and temporal variations in upper mantle viscosity and rheology under Scandinavia. *Geochemistry, Geophysics, Geosystems*, *12*(1).

Caron, L., & Ivins, E. R. (2020). A baseline Antarctic GIA correction for space gravimetry. *Earth and Planetary Science Letters*, *531*, 115957.

Dziewonski, A. M., & Anderson, D. L. (1981). Preliminary reference Earth model. *Physics of the earth and planetary interiors*, *25*(4), 297–356.

Fledmann, J., & Levermann, A. (2015). Collapse of the West Antarctic Ice Sheet after local destabilization of the Amundsen Basin. *PNAS*, *112*, 14191-14196.

Fullea, J., Afonso, J. C., Connolly, J. A. D., Fernàndez, M., García-Castellanos, D., & Zeyen, H. (2009). LitMod3D: An interactive 3D software to model the thermal, compositional, density, seismological, and rheological structure of the lithosphere and sublithospheric upper mantle. *Geochemistry, Geophysics, Geosystems*, *10*(8).

Fullea, J., Lebedev, S., Martinec, Z., & Celli, N. L. (2018). WINTERC: a new Global thermochemical model constrained by seismic waveforms, heat flow, surface elevation and gravity satellite data..

Gasperini, P., Yuen, D. A., & Sabadini, R. (1992). Postglacial rebound with a non-Newtonian upper mantle and a Newtonian lower mantle rheology. *Geophysical Research Letters*, *19*(16), 1711-1714.

Gomez, N., Latychev, K., & Pollard, D. (2018). A Coupled Ice Sheet–Sea Level Model Incorporating 3D Earth Structure: Variations in Antarctica during the Last Deglacial Retreat. *Journal of Climate*, *31*(10), 4041-4054.

Gourmelen, N., Escorihuela, M., Shepherd, A., Foresta, L., Muir, A., Garcia-Mondéjar, A., ... Drinkwater, M. (2018). CryoSat-2 swath interferometric altimetry for mapping ice elevation and elevation change. *Advances in Space Research*, *62*(6), 1226-1242.

Gunter, B., Didova, R., O.and Riva, Ligtenberg, S., Lenaerts, J., King, M., Broeke, M. v. d., & Urban, T. (2014). Empirical estimation of present-day Antarctic glacial isostatic adjustment and ice mass change. *The Cryosphere*, *8*, 743-760.

Hartmann, R., Ebbing, J., & Conrad, P. (2020). A Multiple 1D Earth Approach (M1DEA) to account for lateral viscosity variations in solutions of the sea level equation: An application for glacial isostatic adjustment by Antarctic deglaciation. *Journal of Geodynamics*, *135*.

Hay, C. C., Lau, H. C. P., Gomez, N., Austermann, J., Powell, E., Mitrovica, J. X., ... Wiens, D. A. (2017). Sea Level Fingerprints in a Region of Complex Earth Structure: The Case of WAIS. *Journal of Climate*, *30*(6), 1881-1892.

Hirth, G., & Kohlstedt, D. (2003). Rheology of the upper mantle and the mantle wedge: A view from the experimentalists. *Geophysical Monograph-American Geophysical Union*, *138*, 83-106.

Hu, H., van der Wal, W., & Vermeersen, L. L. A. (2017). A numerical method for reorientation of rotating tidally deformed viscoelastic bodies. *Journal of Geophysical Research: Planets*, *122*(1), 228-248.

Huang, P., Wu, P., & Steffen, H. (2019). In search of an ice history that is consistent with composite rheology in Glacial Isostatic Adjustment modelling", journal = "Earth and Planetary Science Letters. , *517*, 26 - 37.

Ivins, E. R., James, T. S., Wahr, J., O. Schrama, E. J., Landerer, F. W., & Simon, K. M. (2013). Antarctic contribution to sea level rise observed by GRACE with improved GIA correction. *Journal of Geophysical Research: Solid Earth*, *118*(6), 3126-3141.

Johnston, P. (1993). The effect of spatially non-uniform water loads on prediction of sea-level change. *Geophysical Journal International*, *114* (3), 615-634.

Kaufmann, G., Wu, P., & Ivins, E. (2005). Lateral viscosity variations beneath Antarctica and their implications on regional rebound motions and seismotectonics. *Geophysics Journal International*, *161*, 679-706.

Kearey, P., Klepeis, K. A., & Vine, F. J. (2009). *Global Tectonics* (3rd ed.). West Sussex, UK: Wiley–Blackwell.

Kendall, R. A., Mitrovica, J. X., & Milne, G. A. (2005). On post-glacial sea level - II. Numerical formulation and comparative results on spherically symmetric models. *Geophysics Journal International*, *161*, 679-706.

King, M. A., Altamimi, Z., Boehm, J., Bos, M., Dach, R., Elosegui, P., ... Willis, P. (2010). Improved Constraints on Models of Glacial Isostatic Adjustment: A Review of the Contribution of Ground-Based Geodetic Observations. *Surveys in Geophysics*, *31*, 465 - 507.

Kohlstedt, D. (2007). Properties of Rocks and Minerals – Constitutive Equations, Rheological Behavior, and Viscosity of Rocks. In *Treatise on geophysics* (p. 389 - 417). Amsterdam: Elsevier.

Konrad, H., Gilbert, L., Cornford, S. L., Payne, A., Hogg, A., Muir, A., & Shepherd, A. (2016). Uneven onset and pace of ice-dynamical imbalance in the Amundsen Sea Embayment, West Antarctica. *Geophysical Research Letters*, *44* (2), 910-918.

Konrad, H., Sasgen, I., Pollard, D., & Klemann, D. (2015). Potential of the solid-Earth response for limiting long-term West Antarctic Ice Sheet retreat in a warming climate. *Earth and Planetary Science Letters*, *432* (15), 254-264.

Liu, B., King, M., & Dai, W. (2018). Common mode error in Antarctic GPS coordinate time-series on its effect on bedrock-uplift estimates. *Geophysics Journal International*, *214* (3), 1652-1664.

Lloyd, A. J., Wiens, D. A., Nyblade, A. A., Anandakrishnan, S., Aster, R. C., Huerta, A. D., ... Zhao, D. (2015). A seismic transect across West Antarctica: Evidence for mantle thermal anomalies beneath the Bentley Subglacial Trench and the Marie Byrd Land Dome. *Journal of Geophysical Research: Solid Earth*, *120* (12), 8439-8460.

Martinec, Z., Klemann, V., van der Wal, W., Riva, R. E. M., Spada, G., Sun, Y., ... James, T. S. (2018). A benchmark study of numerical implementations of the sea level equation in GIA modelling. *Geophysical Journal International*, *215*, 389-414.

Martín-Español, A., King, M., Zammit-Mangion, A., Andrews, S., Moore, P., & Bamber, J. (2016). An Assessment of Forward and Inverse GIA Solutions for Antarctica. *Journal of Geophysical Research: Solid Earth*, *121*, 6947-6965.

Martín-Español, A., Zammit-Mangion, A., Clarke, P., Flament, T., Helm, V., King, M., … Bamber, J. (2016). Spatial and temporal Antarctic Ice Sheet mass trends, glacio-isostatic adjustment, and surface processes from a joint inversion of satellite altimeter, gravity, and GPS data. *Journal of Geophysical Research: Earth Surface*, *121*, 182-200.

McDonough, W., & Sun, S.-s. (1995). The composition of the Earth. *Chemical Geology*, *120*(3), 223 - 253.

Milne, G. A., & Mitrovica, J. X. (1998). The influence of time-dependent ocean-continent geometry on predictions of post-glacial sea level change in Australia and New Zealand. *Geophysical Research Letters*, *25*(6), 793-796.

Mouginot, J., Rignot, E., & Scheuchl, B. (2014). Sustained increase in ice discharge from the Amundsen Sea Embayment, West Antarctica, from 1973 to 2013. *Geophysical Research Letters*, *41*(5).

Nield, G. A., Barletta, V. R., Bordoni, A., King, M. A., Whitehouse, P. L., Clarke, P. J., … Berthier, E. (2014). Rapid bedrock uplift in the Antarctic Peninsula explained by viscoelastic response to recent ice unloading. *Earth and Planetary Science Letters*, *397*(2), 32-41.

Nield, G. A., Whitehouse, P. L., van der Wal, W., Blank, B., O'Donnell, J. P., & Stuart, G. W. (2018). The impact of lateral variations in lithospheric thickness on glacial isostatic adjustment in West Antarctica. *Geophysics Journal International*, *214*(2), 811-824.

Pappa, F., Ebbing, J., Ferraccioli, F., & van der Wal, W. (2019). Modeling satellite gravity gradient data to derive density, temperature, and viscosity structure of the Antarctic lithosphere. *JGR Solid Earth*, *124*(11).

Peltier, W. (2004). Global glacial isostasy and the surface of the ice-age Earth: The ICE-5G (VM2) Model and GRACE. *Annual Review of Earth and Planetary Sciences*, *32*(1), 111-149.

Powell, E., Gomez, N., Hay, C., Latychev, K., & Mitrovica, J. X. (2020). Viscous effects in the solid Earth response to modern Antarctic ice mass flux: Implications for geodetic studies of WAIS stability in a warming world. *Journal of Climate*, *33*(2), 443-459.

Ranalli, G. (1995). *Rheology of the Earth.* Cambridge University Press.

Samrat, N. H., King, M. A., Watson, C., Hooper, A., Chen, X., Barletta, V. R., & Bordoni, A. (2020, 05). Reduced ice mass loss and three-dimensional viscoelastic deformation in northern Antarctic Peninsula inferred from GPS. *Geophysical Journal International*, *222*(2), 1013-1022.

Schaeffer, A. J., & Lebedev, S. (2013). Global shear speed structure of the upper mantle and transition zone. *Geophysical Journal International*, *194*(1), 417-449.

Schmeling, H. (1987). On the interaction between small- and large-scale convection and postglacial rebound flow in a power-law mantle. *Earth and Planetary Science Letters*, *84*(2), 254 - 262.

Shen, W., Wiens, D. A., Lloyd, A. J., & Nyblade, A. A. (2020). A geothermal heat flux map of Antarctica empirically constrained by seismic structure. *Geophysical Research Letters*, *47*(14), e2020 GL086955.

Shepherd, A., Gilbert, L., Muir, H., Alan S.and Konrad, McMillan, M., Slater, T., Briggs, K. H., ... Engdahl, M. E. (2019). Trends in Antarctic Ice Sheet elevation and mass. *Geophysical Research Letters*, *46*(14), 8174-8183.

Spada, G., Barletta, V. R., Klemann, V., Riva, R. E. M., Martinec, Z., Gasperini, P., ... King, M. A. (2011). A benchmark study for glacial isostatic adjustment codes. *Geophysical Journal International*, *185*(1), 106-132.

van der Wal, W., Barnhoorn, A., Stocchi, P., Gradmann, S., Wu, P., Drury, M., & Vermeersen, B. (2013). Glacial isostatic adjustment model with composite 3-D Earth rheology for Fennoscandia. *Geophysical Journal International*, *194*, 61-77.

van der Wal, W., Whitehouse, P. L., & Schrama, E. J. (2015). Effect of the GIA models with 3D composite mantle viscosity on GRACE mass balance estimates for Antarctica. *Earth and Planetary Sciences Letters*, *414*, 134-143.

van der Wal, W., Wu, P., Wang, H., & Sideris, M. G. (2010). Sea levels and uplift rate from composite rheology in glacial isostatic adjustment modeling. *Journal of Geodynamics*, *50*(1), 38-48.

Whitehouse, P. L., Bentley, M. J., Milne, G. A., King, M. A., & Thomas, I. D. (2012, 09). A new glacial isostatic adjustment model for Antarctica: calibrated and tested using observations of relative sea-level change and present-day uplift rates. *Geophysical Journal International*, *190*(3), 1464-1482.

Whitehouse, P. L., Gomez, N., King, M. A., & Wiens, D. A. (2019). Solid Earth change and the evolution of the Antarctic Ice Sheet. *Nature Communications Volume*, *10*(503).

Wolstencroft, M., King, M. A., Whitehouse, P. L., Bentley, M. J., Nield, G. A., King, E. C., ... Gunter, B. C. (2015). Uplift rates from a new high-density GPS network in Palmer Land indicate significant late Holocene ice loss in the southwestern Weddell Sea. *Geophysical Journal International*, *203*(1), 737-754.

Wu, P. (2001). Postglacial induced surface motion and gravity in Laurentia for uniform mantle with power-law rheology and ambient tectonic stress. *Earth and Planetary Science Letters*, *186*(3), 427-435.

Wu, P. (2004). Using commercial finite element packages for the study of the earth deformations, sea levels and the state of stress. *Geophysics Journal International*, *158*, 401-408.

Zhang, R. (2005). *Numerical Simulation of Solid-state Sintering of Metal Powder Compact Dominated by Grain Boundary Diffusion* (Unpublished doctoral dissertation). Penn State.